

---

1997

# Computer-Aided data acquisition system for a 12" subsonic wind tunnel

Spiros Agelopoulos  
*San Jose State University*

Follow this and additional works at: [https://scholarworks.sjsu.edu/etd\\_theses](https://scholarworks.sjsu.edu/etd_theses)

---

## Recommended Citation

Agelopoulos, Spiros, "Computer-Aided data acquisition system for a 12" subsonic wind tunnel" (1997). *Master's Theses*. 1416.  
DOI: <https://doi.org/10.31979/etd.qdq6-rh5w>  
[https://scholarworks.sjsu.edu/etd\\_theses/1416](https://scholarworks.sjsu.edu/etd_theses/1416)

This Thesis is brought to you for free and open access by the Master's Theses and Graduate Research at SJSU ScholarWorks. It has been accepted for inclusion in Master's Theses by an authorized administrator of SJSU ScholarWorks. For more information, please contact [scholarworks@sjsu.edu](mailto:scholarworks@sjsu.edu).

## INFORMATION TO USERS

This manuscript has been reproduced from the microfilm master. UMI films the text directly from the original or copy submitted. Thus, some thesis and dissertation copies are in typewriter face, while others may be from any type of computer printer.

**The quality of this reproduction is dependent upon the quality of the copy submitted.** Broken or indistinct print, colored or poor quality illustrations and photographs, print bleedthrough, substandard margins, and improper alignment can adversely affect reproduction.

In the unlikely event that the author did not send UMI a complete manuscript and there are missing pages, these will be noted. Also, if unauthorized copyright material had to be removed, a note will indicate the deletion.

Oversize materials (e.g., maps, drawings, charts) are reproduced by sectioning the original, beginning at the upper left-hand corner and continuing from left to right in equal sections with small overlaps. Each original is also photographed in one exposure and is included in reduced form at the back of the book.

Photographs included in the original manuscript have been reproduced xerographically in this copy. Higher quality 6" x 9" black and white photographic prints are available for any photographs or illustrations appearing in this copy for an additional charge. Contact UMI directly to order.

# UMI

A Bell & Howell Information Company  
300 North Zeeb Road, Ann Arbor MI 48106-1346 USA  
313/761-4700 800/521-0600



COMPUTER-AIDED DATA ACQUISITION SYSTEM  
FOR A 12" SUBSONIC WIND TUNNEL

A thesis

Presented to

The Faculty of the Department of Aerospace Engineering

San Jose State University

In Partial Fulfillment

of the Requirements for the Degree

Master of Science

by

Spiros Agelopoulos

May 1997

**UMI Number: 1384665**

---

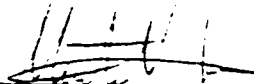
**UMI Microform 1384665**  
**Copyright 1997, by UMI Company. All rights reserved.**

**This microform edition is protected against unauthorized  
copying under Title 17, United States Code.**

---


**UMI**  
**300 North Zeeb Road**  
**Ann Arbor, MI 48103**

APPROVED FOR THE DEPARTMENT OF AEROSPACE  
ENGINEERING MSAE PROGRAM



---

Dr. Nikos Mourtos  
Project Advisor  
Aerospace Engineering, SJSU



---

Dr. Dick Desautel  
Chairman  
Aerospace Engineering, SJSU



---

Francis Richason  
Sterling Software, NASA Ames Research Center

APPROVED FOR THE UNIVERSITY



---

© 1997

Spiros Agelopoulos

ALL RIGHTS RESERVED

## ABSTRACT

### COMPUTER-AIDED DATA ACQUISITION SYSTEM FOR A 12" SUBSONIC WIND TUNNEL

By Spiros Agelopoulos

The concept of automatic data acquisition and processing was applied to the 12" subsonic wind tunnel at San Jose State University's Aerospace Engineering Department's facilities. Pressure transducers, position indicators, a dynamometer and a pitot tube traversing assembly were used to capture physical measurements. Their output signals were converted by a multichannel digital to analog board which, in turn, routed the data to LabVIEW for further processing. Processing included the creation of virtual instruments that automatically manipulated data to illustrate phenomena of interest to the field of aerodynamics. In addition to the construction and programming of the interface, several example virtual instruments were created, and the results of their operation were within reasonable error from sophisticated large-scale data acquisition systems. Experience was also gained from the use of a two-dimensional aerodynamic airflow simulation program and its use was analyzed.



## Please Note

Page(s) missing in number only; text follows.  
Filmed as received.

v

UMI

## **Acknowledgments**

I would like to give special thanks to all those people, from both NASA and San Jose State University, who contributed to the creation of the data acquisition system. In particular, I wish to express my appreciation to Dr. Nikos Mourtos for his consistent feedback, and to the students of the undergraduate class AE 162 who were the beta testers of the setup.

# Table of Contents

<b>CHAPTER 1 INTRODUCTION</b> -----	<b>1</b>
1.1 MOTIVATION.....	1
1.2 PREVIOUS WORK.....	1
1.3 PRESENT APPROACH.....	2
<b>CHAPTER 2 WIND TUNNEL INSTRUMENTATION</b> -----	<b>3</b>
2.1 WIND TUNNEL APPARATUS.....	3
2.2 INSTRUMENTATION.....	3
2.3 METER CABINET.....	4
2.4 PRESSURE TRANSDUCER.....	6
2.5 DYNAMOMETER ASSEMBLY.....	6
2.6 PROBE TRAVERSING ASSEMBLY.....	7
2.7 STANDARD TEST SECTION FEATURES.....	8
<b>CHAPTER 3 DATA ACQUISITION HARDWARE</b> -----	<b>9</b>
3.1 PRESSURE TRANSDUCERS.....	9
3.2 CONNECTOR BLOCK.....	11
3.3 DAQ I/O BOARD.....	11
<b>CHAPTER 4 INTRODUCTION TO LABVIEW</b> -----	<b>13</b>
4.1 BACKGROUND.....	13
4.2 APPLICATION DEVELOPMENT.....	13
4.3 MODULAR DESIGN.....	15
4.4 DATA ACQUISITION.....	15

<b>CHAPTER 5 BUILDING BLOCKS</b> .....	<b>17</b>
5.1 BASIC LABVIEW VIS.....	17
5.2 PROCESSING ALGORITHMS.....	19
<b>CHAPTER 6 WIND TUNNEL VELOCITY PROFILE</b> .....	<b>21</b>
6.1 THEORY.....	21
6.2 VI LOGIC.....	21
6.3 WAKE DRAG.....	23
6.4 EXPERIMENTAL/VALIDATION RESULTS.....	24
<b>CHAPTER 7 MULTIPLE CONSOLE OUTPUT</b> .....	<b>25</b>
7.1 THEORY.....	25
7.2 VI LOGIC.....	26
7.3 EXPERIMENTAL/VALIDATION RESULTS.....	27
<b>CHAPTER 8 PRESSURE COEFFICIENTS FOR NACA 4412</b> .....	<b>29</b>
8.1 THEORY.....	29
8.2 VI LOGIC.....	30
8.3 EXPERIMENTAL/VALIDATION RESULTS.....	49
<b>CHAPTER 9 SUB2D</b> .....	<b>33</b>
9.1 INTRODUCTION.....	33
9.2 FEATURES.....	33
9.3 INTEGRATION WITH LABVIEW.....	36
9.4 RESULTS.....	36
<b>CHAPTER 10 CONCLUSIONS AND RECOMMENDATIONS</b> .....	<b>37</b>
10.1 CONCLUSIONS.....	37
10.2 RECOMMENDATIONS.....	37

<b>REFERENCES</b> .....	<b>40</b>
<b>FIGURES</b> .....	<b>41</b>
<b>APPENDIX A</b> .....	<b>62</b>
LABVIEW FUNCTIONS.....	.62
<b>APPENDIX B</b> .....	<b>64</b>
LABVIEW MANUAL FOR AE 162 LABORATORY .....	.64
INTRODUCTION TO LABVIEW FOR STUDENTS .....	.64
STARTING LABVIEW .....	.65

## Nomenclature

### Letter symbols

$\frac{x}{c}$	percent of chord
A	unit of electrical current - amp
$\alpha$	angle of attack
$a_{L=0}$	zero lift angle of attack
$c_d, C_d$	coefficient of drag
$c_l, C_l$	coefficient of lift
$c_m$	coefficient of moment
$c_p, C_p$	coefficient of pressure
D	drag
fps	unit of speed - feet per second
g	gravitational acceleration (9.81 m/s <sup>2</sup> )
G	graphical programming language
L	lift
lbf	unit of force - pounds
m/s	unit of speed - meters of second
Nt	unit of force - Newtons (SI)
psi	unit of pressure - pounds per square inch
S	samples
V	unit of electrical differential potential - volt

## **Abbreviations**

<b>AD</b>	Analog to Digital
<b>AC</b>	Alternating Current
<b>AI</b>	Analog Instrument
<b>CPU</b>	Central Processing Unit
<b>DAQ</b>	Data Acquisition
<b>DC</b>	Direct Current
<b>DDE</b>	Dynamic Data Exchange
<b>DIP</b>	Dual Inline Package - Binary signal switch
<b>DLL</b>	Dynamic Link Library
<b>ELD</b>	Engineering Laboratory Design
<b>FSO</b>	Full Scale Output
<b>ftp</b>	File Transfer Protocol
<b>GPIB</b>	General Purpose Interface Bus
<b>GUI</b>	Graphical User Interface
<b>I/O</b>	Input/Output
<b>IP</b>	Internet Protocol
<b>L/D</b>	Lift over Drag
<b>LED</b>	Light Emitting Diode
<b>LVDT</b>	Linear Variable Differential Transformer
<b>NACA</b>	National Aeronautics Committee on Aeronautics
<b>NAND</b>	Inverted AND Gate
<b>NASA</b>	National Aeronautics and Space Administration
<b>NATINST</b>	National Instruments
<b>OLE</b>	Object Linking Extensions

PANDA	Flow Visualization Software
PLC	Programmable Logic Controller
SI	Système International
TCP	Transmission Control Protocol
UDP	User Datagram Protocol
VI	Virtual Instrument
VXI	VME Bus Extension for Instrumentation



## List of Figures

FIGURE 2.1: 12" WIND TUNNEL .....	41
FIGURE 2.2: ELD METER CABINET .....	41
FIGURE 2.3: METER CABINET CALIBRATION CONTROLS .....	42
FIGURE 2.4: TEST SECTION WITH NACA 4412 AND DYNAMOMETER.....	42
FIGURE 2.5: WIND TUNNEL DIMENSIONS .....	43
FIGURE 3.1: PRESSURE TRANSDUCER ARRAY .....	44
FIGURE 3.2: POWER AND GROUND DISTRIBUTION, AND POWER SUPPLY .....	45
FIGURE 3.3: SCB-100 WIRING DIAGRAM.....	46
FIGURE 3.4: SCB-100 LAYOUT .....	47
FIGURE 5.1: X-POS.VI - X-POSITION SUBROUTINE.....	48
FIGURE 5.2: PITOT.VI - PITOT TUBE SUBROUTINE.....	49
FIGURE 6.1: EXAGGERATED FLOW BEHAVIOR INSIDE A WIND TUNNEL'S TEST SECTION .....	50
FIGURE 6.2: FLOW QUALITY MEASUREMENT MATRIX .....	50
FIGURE 6.3: X,Y.VI - FIXED POSITION VELOCITY MEASUREMENT.....	51
FIGURE 6.4: AIR VELOCITY MATRIX - 30 POINTS.....	52
FIGURE 6.5: WAKE DRAG SETUP .....	53
FIGURE 7.1: CONSOLE.VI - LIFT AND DRAG COMPONENTS .....	54
FIGURE 8.1: CP4412.VI - CP CALCULATIONS .....	55
FIGURE 8.2: CP4412.VI AT 0M/S.....	56
FIGURE 8.3: TEST SECTION WITH NACA 4412 AND TUBING.....	57

FIGURE 9.1: SUB2D OUTPUT - CP DISTRIBUTION AT $M = 0.12$ , $\alpha = 0^\circ$ .....	58
FIGURE 9.2: SUB2D OUTPUT - CP DISTRIBUTION AT $M = 0.12$ , $\alpha = 15^\circ$ .....	59
FIGURE 9.3: SUB2D OUTPUT - CL VS. $\alpha$ AT $M = 0.12$ .....	60
FIGURE 9.4: SUB2D OUTPUT - CD VS. $\alpha$ AT $M = 0.12$ .....	61

## List of Tables

TABLE 2.1: SIGNAL ROUTING FROM THE METER CABINET.....	5
TABLE 2.2: WIND TUNNEL INSTRUMENTATION RANGES.....	7
TABLE 3.1: PX 143D $\pm 5$ PSI SPECIFICATIONS.....	10
TABLE 3.2: I/O BOARD SPECIFICATIONS.....	12
TABLE 6.1: DRAG MEASUREMENTS FOR NACA 4412 AT 50 M/S, $\alpha = 4^\circ$ .....	24
TABLE 7.1: DRAG MEASUREMENTS FOR VARIOUS MODELS 4412 AT 52 M/S.....	28
TABLE 8.1: VALIDATION RESULTS.....	32

## **Chapter 1 : Introduction**

### **1.1 Motivation**

The dramatic increase in the performance of today's computers has resulted in the creation of a variety of scientific and engineering software that provide quick, repeatable and reliable functionality in many laboratory environments. These computers have replaced many traditional tools and methods, and have provided the ability to monitor and act on various experiments in a way that, 10 years ago, would have required tremendously more expensive and massive computer resources.

Using a DAQ system, students can learn about many aspects of airflow behavior and its effect on aerodynamic bodies. They can observe and collect data faster than with traditional methods (paper and pencil), and they can practice with laboratory environments that simulate the larger sophisticated ones they will encounter in the industry.

### **1.2 Previous Work**

The aerodynamics facility in San Jose State University's Aerospace Engineering department consisted of a 12" wind tunnel and its associated set of sensors (such as a dynamometer and its control cabinet). Although the setup had the capability of interfacing with a computer, proper computing tools were not available when the system was originally installed.

Students had to use inconsistent tools to collect data, and at times were unable to capture the correct values due to rapidly changing conditions. Computer-aided tools were not available on the scale required for use in a university laboratory environment.

### **1.3 Present Approach**

The concept of using computers in DAQ applications is not new. However, using them in a cost effective manner and in simple to moderate applications is the result of National Instruments' development of LabVIEW. LabVIEW is a sophisticated program that can be easily adapted to many laboratories' needs and can provide not only real-time monitoring but also the ability to simulate physical conditions.

The work of my thesis consisted of four parts:

1. Design and setup of necessary hardware (sensors) and software (LabVIEW, Sub2D)
2. Installation and configuration of hardware and software
3. Test validation
4. Field implementation (use in classrooms)

## **Chapter 2 : Wind Tunnel Instrumentation**

### **2.1 Wind Tunnel Apparatus**

The ELD 12" wind tunnel is an open-circuit type powered by a 10 hp electric motor. When activated, the motor pulls the air and rotates at a constant 3,600 rpm. The airspeed inside the tunnel is controlled by varying the gap upstream from the fan section, and downstream from the test section. As the fan is attached to the front of the diffuser, the whole assembly can move in unison. This, combined with the airflow settling chamber, provide a smooth and uniform airflow in the test section, with the air undisturbed from airspeed adjustment mechanisms (Figures 2.1, 2.5).

### **2.2 Instrumentation**

The ELD wind tunnel instrumentation system is a complete basic-instrument package which has been designed for use with subsonic wind tunnels in undergraduate student laboratories. Its functions include the measurements of lift and drag forces, the measurements of static and dynamic pressures, and the reporting of the axial and vertical position (x and y coordinates) of a traversing probe. The system consists of three major components: the meter cabinet, the dynamometer assembly, and the probe traversing assembly.

### 2.3 Meter Cabinet

The meter cabinet contains a printed circuit board, a DC power supply, two signal conditioner chips for lift and drag, a pressure transducer, and a DC-voltage digital panel meter (which contains the readout screen). The front of the panel includes a mode selector, through which a user can select what will be displayed on the single-parameter readout screen, and the power switch [1]. At any time, the user can monitor the x- or y-axis position of the traversing assembly, the pressure at either the pitot tube or one of the pressure ports, and the lift and drag components (Figure 2.2). The back of the cabinet is fitted with a clear Plexiglas panel, on which calibration potentiometers and DIP switches are mounted. These control the reference and span points for each physical variable, as well as the position of the decimal point on the four-digit display. The option to change the decimal point position assists the user in displaying measurements in any meaningful engineering units by shifting it appropriately (Figure 2.3).

Although the digital display can only handle one readout at a time, the back of the panel features a 12-pin female port from which a user can collect all measurements simultaneously in the selected engineering units (Table 2.1). The analog signals from the cabinet are routed to the signal conditioning box (Chapter 3).

**Table 2.1: Signal routing from the meter cabinet**

<b>Pin #</b>	<b>Function</b>	<b>Cable color<sup>1</sup></b>
1	Pressure	Solid white
2	Lift	White with black stripe
3	Drag	Green with black stripe
4	x-position	Solid green
5	y-position	Blue with white stripe
6	Not used	Orange with green stripe
7	Ground for pressure	Blue with red stripe
8	Ground for lift	Blue with black stripe
9	Ground for drag	Solid blue
10	Ground for x-position	Orange with black stripe
11	Ground for y-position	Solid stripe
12	Not used	Orange with red stripe

<sup>1</sup> Cable color refers to the color of the cable that carries the respective signal to the conditioning box.



## **2.4 Pressure Transducer**

The differential-type pressure transducer consists of a precision pressure capsule; an LVDT; and excitation, demodulation, and amplification circuitry. Pressure is applied to the sealed cavity surrounding the pressure capsule. The reference pressure, either atmosphere or the test section static pressure, is applied to the interior of the capsule. The capsule deflects linearly in response to the differences in the applied pressures. The movable core of the LVDT is coupled to the pressure capsule and is translated within the LVDT armature as the capsule deflects. The resulting output voltage from the LVDT is proportional to the applied differential pressure.

## **2.5 Dynamometer Assembly**

The dynamometer is a two-component device designed to measure lift and drag forces. It is mounted on the external side of the floor of the test section. It uses two pairs or restrained, cantilevered beams separated by one spacer block for each axis. Forces generated by a model under test conditions are conveyed to the dynamometer via a stiff strut and result in the deflection of the beam assemblies. These deflections are proportional (within range) to the magnitude of the applied forces. The deflection of each beam assembly is sensed by an LVDT (the armature moves with the deflecting beam, and the core is fixed to the base block but is adjustable for zeroing). Output voltage signals from the LVDT are demodulated and amplified by signal-conditioning circuits. The resulting DC voltages represent the direction and magnitude of the applied forces and may be calibrated

to readout in any desired engineering units, i.e., lbf, Nt, etc. An aerodynamic teardrop shroud shields the major portion of the force strut from the air stream.

**Table 2.2: Wind tunnel instrumentation ranges**

Test section dimensions	12" by 12"
Maximum speed with closed gap	150 fps
Pressure transducer range	-10" H <sub>2</sub> O to 10" H <sub>2</sub> O differential
Maximum lift	8 lbf
Maximum drag	5 lbf

## **2.6 Probe Traversing Assembly**

The two-axes probe traversing mechanism is capable of positioning and reporting the location of a probe at any point in the upstream 75% of the test section vertical centerline plane [1]. The device is driven manually via two hand wheels and precision, high helix, aluminum-lead screws running in polyurethane nuts. Minimal backlash is a characteristic of the drive system. Precision potentiometers are secured to the drive screws and report the location of the probe in each axis. The voltage signal from each potentiometer is transmitted to the meter cabinet. The probe can be traversed from the floor to the ceiling and may be withdrawn through the neoprene seal in the cover slot. Longitudinal traversing begins near the upstream face of the test section. Its travel downstream is limited only by the horizontal dimension of the probe support assembly. The system also includes two heads, one for boundary layer measurements and one for the pitot tube used throughout the LabVIEW-based setup.

## **2.7 Standard Test Section Features**

The test section cover is removable and mounts the traversing assembly. Quick-release fasteners align and secure the cover to the test section. Both front sidewalls include a 4" access port, which allow for some rotation of the models if they are attached to these sides. The port is closed during operation by a flanged Plexiglas plug. Several of the models use dedicated plugs as mounting fixtures. A degree-indexed scale surrounds the port. Stainless-steel thumb screws secure the plug in the port. An aperture is provided in the test section floor for mounting the dynamometer. A Plexiglas plate with an insert closes the opening when the dynamometer is removed (Figure 2.4).

## **Chapter 3 : Data Acquisition Hardware**

### **3.1 Pressure Transducers**

The pressure array is comprised of 15 Omega PX143 differential pressure transducers. One of these transducers measures the pressure difference between the wind tunnel and the room. The remaining transducers measure the pressure difference between taps on an airfoil's surface and the wind tunnel test section (Figure 3.1). These transducers are manufactured by Microswitch and distributed by Omega Engineering. They use a solid-state piezoelectric mechanism that ensures exact measurement of pressure, low hysteresis, and long-term stability. Special circuitry to provide temperature compensation is an integral part of the device, and is optimized on each unit as part of the initial calibration procedure. Null and full-scale output are similarly controlled during factory calibration. The transducers do not require any additional calibration, unless there is a general malfunction by the device.

Pressure is sensed through a diaphragm with implanted resistors. Pressure applied on the diaphragm causes it to flex and the resistance to change, resulting in an output voltage proportional to pressure. This feature ensures predictable output over a variety of conditions. The circuitry is contained in a thermoplastic housing with printed circuit terminals exiting on the opposite side from the sensing ports.

Two sets of six and one set of three pressure transducers are mounted inside special plastic project boxes (Figure 3.1). Each box has its own power source and ground connect. All

transducers in each box are connected to the power and ground strips. Custom connectors to each transducer ensure signal and ground isolation in an easily replaceable module. Power and ground connections to the three boxes are provided externally through a dedicated 12 Volt power supply and two distribution devices (Figure 3.2).

**Table 3.1: PX 143D  $\pm 5$  psi specifications**

<b>Performance parameters</b>	<b>Value</b>
Overpressure, max.	15 psi
Hysteresis and repeatability, typ.	$\pm 0.15$ %F.S.O. ( $\pm 0.15$ psi)
Linearity (P2 > P1)	0.07psi
Linearity (P1 < P2)	0.04psi
Response time	1msec
Stability over one year	$\pm 05$ psi
Shock	Qualification tested to 50g, 11msec, half sine
Vibration	Qualification tested to 10g sine
Media compatibility (P1)	Dry gas
Media compatibility (P2)	Media compatible with polyester, silicone
Short circuit protection	Output may be sorted indefinitely
Ground reference	Supply and output are common
<b>Setup parameters</b>	<b>Value</b>
Excitation	12V
Supply current	8mA
Output min	1.5V
Output max	9V

### **3.2 Connector Block**

The SCB-100 is a shielded I/O connector block made by National Instruments for interfacing I/O signals to the DAQ board. All signals to be processed by the DAQ terminate on this block. It is designed to provide rugged, very low-noise signal termination—a characteristic enhanced by the use of the shielded cable. The block uses screw terminals for easy connection of voltage and current signals. Although the normal setup does not use any temperature sensors (such as thermocouples), it includes a special temperature-compensating element for cold-junction compensation and general-purpose breadboard areas. The block can accommodate up to 64 channels (0-63) and can condition voltage or current signals. Although the block can provide +5V from the DAQ board to power sensors that require external power supply, it can also accommodate third-party supplies for even greater flexibility. Figure 3.3 illustrates the connections on the SCB-100, and Figure 3.4 shows the actual wiring clusters on the same block.

### **3.3 DAQ I/O Board**

The conditioned signals arrive at the computer via a shielded 100-pin cable and are handled by a National Instruments AT-MIO-64E-3 multifunction PnP I/O board for the ISA data bus. All addresses, including the base I/O address, are handled by software, avoiding the need for DIP or other switches. The board can process signals referenced at floating or preset grounds, and can accept as inputs either single channels or pairs of channels for differential measurements.

**Table 3.2: I/O board specifications**

<b>Technical specifications</b>	<b>Value</b>
Sampling rate	600kS/s
Maximum number of single-ended channels	64
Maximum number of differential channels	32
DA converter depth	12bit
I/O timer	2x24bit
Maximum resolution	50ns

## **Chapter 4 : Introduction to LabVIEW**

### **4.1 Background**

LabVIEW was introduced in 1986 when it pioneered a new instrumentation approach called Virtual Instrumentation [2]. VI allows users to build their own instrumentation systems with standard computers and hardware. These software-centered systems leverage off the computational, display, and connectivity capabilities of popular computers to provide the power and flexibility to build countless instrumentation functions.

By combining LabVIEW with standard data acquisition and instrument-control devices, a programmer can create virtual instruments and use them in many applications. Unlike traditional instruments, which are limited by the design of the manufacturer, a virtual instrument can operate as a variety of devices, such as a temperature monitor, voltmeter, strip-chart recorder, digitizer, and signal analyzer, or as in the case of the 12" wind tunnel, it can operate as a general-monitoring and data-collecting system.

### **4.2 Application Development**

LabVIEW eases application development with Graphical User Interface (GUI) libraries, analysis libraries, and I/O libraries for GPIB, VXI, DAQ, and serial interfaces (Appendix A). In addition, the user can easily connect to other applications through networking and



inter-application communication. LabVIEW also offers an open architecture with which the user can call any DLL or shared code and libraries.

Unlike traditional text-based programming languages, LabVIEW uses a graphical programming language – G – to create programs in block diagram form. This feature makes LabVIEW easy to program since the main interface consists of terminology, icons, and ideas familiar to engineers, and describes programming actions symbolically. The data flow used by G naturally represents application functions, such as data analysis, high-speed data acquisition, and advanced control algorithms.

When programming on LabVIEW the programmer builds VIs instead of writing programs. The first element is the external interface, the front panel, for interactive control. This is followed by specifying the functionality of elements on the front panel and assembling the logic block diagram. Palettes and pull-down menus supply all interface and block-diagrams. They are grouped by function and environment and include numeric displays, meters, gauges, thermometers, tanks, LEDs, charts, graphs etc. When the VI is complete, the front panel is used to control the system, while the VI is running, by clicking a switch, moving a slide, zooming in on a graph, or entering a value from the keyboard.

The graphical-block diagram is constructed without worrying about the many syntactical details of conventional programming. Objects (icons) from the Functions palette are connected with wires to pass data from one block to the next. These blocks range from simple arithmetic functions, to advanced acquisition and analysis routines, to network and file I/O operations. LabVIEW uses a patented data-flow programming model that departs from the linear architecture of text-based languages. Because the execution order in LabVIEW is determined by the flow of data between blocks and not by sequential lines of

text, diagrams can be created describing simultaneous operations. Consequently, LabVIEW is a multitasking system, running multiple execution threads and multiple VIs.

### **4.3 Modular Design**

LabVIEW VIs are modular in design, so any VI can run by itself or be used as part of another VI. VI properties such as representative icons can be created and grouped. Basic VIs that perform aerodynamic and project-specific functionality are described in Chapter 5. The programmer can design a hierarchy of VIs and sub-VIs that can be modified, interchanged, and combined with other VIs to meet various application needs. The graphical compiler offers critical execution speed. LabVIEW is the only graphical programming system with a compiler that generates optimized code with execution speeds comparable to compiled C programs. A built-in profiler can analyze and optimize time-critical sections of graphical code.

### **4.4 Data Acquisition**

The DAQ VI Library has functions to acquire and output data with all National Instruments plug-in and remote DAQ peripherals, such as the DAQ I/O board used in the wind tunnel setup [3]. LabVIEW also has drivers for industrial I/O devices, such as PLCs, data loggers, and single-loop controllers. Data collected can be processed via LabVIEW's powerful, comprehensive analysis libraries which are complete with statistics, evaluations, regressions, linear algebra, signal generation algorithms, time and frequency-domain algorithms, windowing routines, and digital filters. LabVIEW features numerous VI

Libraries to communicate with other applications as well. Using CodeLink, one can automatically share C libraries developed in LabWindows/CVI, National Instrument's application development tool for C programming. TCP/IP and UDP networking VIs can be used to communicate with remote applications. The Internet toolkit interfaces e-mail, ftp, and web capabilities to DAQ applications. With remote automation VIs, a user can control the execution of distributed VIs on remote machines.

## Chapter 5 : Building Blocks

### 5.1 Basic LabVIEW VIs

All physical measurements made by the sensors are converted into voltage signals whose amplitude is linearly proportional to the respective changing conditions. Typically sensors do not produce more than 10 Volts output at maximum range if the excitation voltage is within the manufacturer's recommendations. This is not a concern for the console's analog output since it is regulated by the ELD's electronic design. The pressure transducers, however, use an excitation source which is 50% higher than normal (12 Volts versus 8 Volts typical and 16 Volts maximum). This increases the output range from 1 Volt minimum, 6 Volts maximum, to 1.5 Volts minimum, 9 Volts maximum. The gain from using higher excitation voltage is twofold:

1. Electronic sensitivity is increased by 50%. The 10 psi range is spread across 7.5 Volts instead of the normal 5 Volts, allowing for more precise A/D conversion by the conditioning board.
2. Power supply availability is improved. 12 Volt power supplies are common AC/DC voltage converters making replacement easier (when necessary).

The DAQ I/O board is set to process voltage ranges from 0 Volts to 10 Volts.

After each signal is converted on a hardware level from analog to digital, it becomes available to the controlling software. Several VIs and sub-VIs were used to process each signal. The most basic programming unit is the AI Config VI. The AI Config VI configures an analog input operation for a specified set of channels. It configures the

hardware and allocates a buffer for a buffered analog-input operation. It consists of several advanced analog input VIs which are called to set up a task for a buffered analog-input acquisition. The AI Config VI calls the AI Group Config VI for the specified device (A/D board), group, and channels to create a taskID. It then calls the AI Hardware Config VI to record information about the hardware configuration. The *input limits* input passes to the AI Hardware Config VI, which sets the lower and upper voltage limits for each channel. This VI configures the number of A/D boards, the coupling used for each channel (AC, DC, ground, or internal reference), and the input configuration (differential, reference single-ended, or non-referenced single-ended, which is used throughout this setup).

The AI Config VI configures the buffer for the acquisition by calling the AI Buffer Config AI. This VI allocates memory for the specified number of buffers (set at one per channel), while each buffer contains 1000 scans at a time. The speed at which these scans are acquired is dependent on the host computer's specifications, including CPU speed, bus speed, bus interface, and hard drive type.

The functionality of the AI Config VI is embedded in the AI One Pt VI's functionality. This VI performs a single voltage reading from a specified channel, and monitors error conditions. If an error occurs, the user is given specific information to correct the problem.

## 5.2 Processing Algorithms

The AI One Pt VI's capabilities are used in creating the following sub-VIs which are used throughout the wind tunnel setup:

1. X-POS.VI: The signal from pin 72 of the SCB-100 board (channel 42) is processed by the A/D board and manipulated by the AI One Pt VI. The output from this VI is multiplied by 10 to match the value that is ordinarily shown on the console's display. The output is then relayed directly to a numerical indicator on the front panel's screen (Figure 5.1). The same algorithm processes the Y-POS.VI, whose input is from the y-axis movement of the traversing probe assembly. The output signal from the probe is relayed by the console to pin 73 (channel 35) of the SCB-100.
2. PITOT.VI: The signal from pin 69 of the SCB-100 board (channel 33) is processed by the A/D board and manipulated by the AI One PT VI. The output from this VI is processed according to the formula:

$$V = \sqrt{\frac{2(p_o - p)}{\rho}} \quad (5.1)$$

where  $\rho = 1.23 \frac{kg}{m^3}$  and  $(p_o - p)$  is the signal from the AI One Pt VI, also known as the dynamic pressure measured by the pitot tube [4]. For simplicity and to maximize the efficiency of the code (and as such, the speed of the compiled VI), the constants under the square root are multiplied directly to the square root of the dynamic pressure. The constant also performs unit conversion since the dynamic pressure indicated by the console is in

inches of H<sub>2</sub>O and the desired units for the air velocity at the pitot tube should be in m/s (Figure 5.2). The constant is calculated as follows:

$$\sqrt{\frac{2 \cdot 248.84 \frac{Pa}{inH_2O}}{1.23 \frac{kg}{m^3}}} = 20.12 \frac{m}{s} \quad (5.2)$$

## **Chapter 6 : Wind Tunnel Velocity Profile**

### **6.1 Theory**

The conditions inside the test section of the wind tunnel can be approximated to those of steady and laminar viscous flow between fixed parallel plates. The fluid particles move only in the x-direction, parallel to the plates, and there is no velocity in the y and z directions. The viscous properties of air change the shape of the profile from that of a straight line to a slightly parabolic shape (Figure 6.1). The VEL-PROF.VI discussed below was designed to graphically illustrate the magnitude of air velocity at 30 different points inside the test section, as shown in Figure 6.2. The velocity profile can illustrate both the flow qualities for the empty test section as well as provide data for the computation of drag from various airfoils on the test support (dynamometer).

### **6.2 VI Logic**

The VEL-PROF.VI uses the output from the three main sub-VIs: the X-POS.VI, Y-POS.VI, and PITOT.VI. Each of the 30 points inside the wind tunnel operate with duplicate sets of these VIs. The only difference among them are the pre-programmed two-dimensions Cartesian coordinates that correspond to each point (since the traversing probe assembly moves only on the x and y axes, there is no provision for the z axis).



Although the coordinates can be displayed in any engineering units, this discussion assumes that the coordinates are displayed in inches. The thirty points are then divided in three x-axis points and ten y-axis points that create the desired matrix. The first point is assumed to be at  $(x_1, y_1)=(1'', 0.5'')$  and the 30th at  $(x_3, y_{10})=(22'', 11.5'')$ .

A screen-recording mechanism was devised to correct LabVIEW's lack of capability to retain values on the front panel while the associated inputs are being updated (Figure 6.3). Let us assume that the user wants to measure the airspeed at point at  $(x_1, y_1)$ . The input from the X and Y-POS.VI is subtracted from the prescribed coordinates at this point (X-POS - 1'') and (Y-POS - 0.5''). This computes the deviation of the traversing probe from the desired point. The probe may be ahead, behind, above or below the desired point and as such the difference computed may be a positive or negative number. Of interest is the absolute value of the deviation, and it is computed immediately after the difference computation. The difference is then compared against the acceptable margin of error of the probe's current position from the desired position. If the absolute value is greater than the margin of error, then the comparison module returns a Boolean 1. A NAND logic gate then processes the Boolean results from the two coordinates. The NAND gate returns the Boolean 1 when both X and Y-POS calculations have verified that the traversing probe is within acceptable limits from the particular point. This algorithm is embedded inside a logical *while* loop. It is a loop which allows all processes within to be active continuously, but restricts passing arguments outside, on whether the conditional variable is set to 1 (thus allowing values to exit the loop), or 0 (thus prohibiting values from exiting the loop). The conditional variable is controlled by the output from the NAND gate. The third sub-VI inside the loop is the PITOT.VI which constantly computes the air velocity. When the while loop has received a 1, it allows the pitot tube's airspeed to exit the loop and be displayed on the front panel. While the probe is within the margin of error for the specified

coordinate, the speed is updated on the front panel every 1/100th of a second (the approximate value of which depends on CPU loads). When the user moves the probe appreciably, the airspeed at the particular point ceases getting updated on the front panel. This allows for the speeds to remain on the screen graphically until the user decides to end the laboratory (Figure 6.4).

When the user passes the probe over all 30 points, he can then print the resulting array of velocity magnitudes, and visually inspect the velocity profile at three different cross sections of the wind tunnel.

### **6.3 Wake Drag**

Using data collected from the velocity profile VI, the user can calculate the total drag for an airfoil at a particular air-stream velocity. Plotting the velocity at each point and integrating the area between the lines that connect these points gives the value of the drag force [5]. The drag computed with this method can be compared with that measured by the dynamometer under the same conditions. Table 6.1 illustrates the results from these two methods for the NACA 4412 airfoil and Figure 6.5 illustrates the experimental layout.

## 6.4 Experimental/Validation Results

**Table 6.1: Drag measurements for NACA 4412 at 50 m/s,  $\alpha=4^\circ$**

Drag calculated by the airfoil's wake speeds:	1.276 Nt
Drag measured by the dynamometer:	1.273 Nt
Difference:	0.2%

Data collected

Y-POS (cm)	Wake speed (m/s)
2.5	49.5
9.6	49.6
11.8	49.7
11.9	49.7
12.1	49.1
12.2	48.4
12.3	47.1
12.4	45.9
12.6	45.5
12.8	45.7
13.0	47.0
13.2	48.6
13.5	49.6
22.8	49.9

## **Chapter 7 : Console Multiple Output**

### **7.1 Theory**

The meter cabinet's analog output includes the lift and drag signals from the dynamometer. These can be used to study the properties of various models, including flat plates and airfoils at various angles of attack, as well as simple objects such as smooth- and rough-surface spheres. For lifting models, an additional property of interest is the lift to drag ratio ( $L/D$ ). Many aspects of the performance of an airfoil or flight vehicle are directly related to this ratio. Keeping other physical parameters equal, higher  $L/D$  indicates better flight performance. Airfoils typically exhibit high  $L/D$  values since their function is to produce lift with as little drag as possible.

## 7.2 VI Logic

The CONSOLE.VI also uses the output from the three main sub-VIs: the X-POS.VI, Y-POS.VI and PITOT.VI. The values from these sub-VIs are displayed directly on the front panel of the VI without any additional manipulation. The only adjustment is for optionally setting the reference point for the traversing probe assembly to assist in determining the location at which velocity measurements are taken. To zero the probe's location, the user must first type a zero for the adjustment factor for the two coordinate sub-VIs. This will automatically display the probe's offset values from the desired reference point. Typing these values in the offset cells automatically subtracts the offset from each measured position, thus allowing for measurements from the specified reference point.

The meter cabinet also has outputs for the lift and drag components from the dynamometer. Each raw lift and drag signal is converted to engineering units via the following equation:

$$y = m \cdot x + b \quad (7.1)$$

where  $x$  is the raw signal from each measurement,  $y$  is the same signal converted to engineering units, and  $m$  and  $b$  are the constants that determine the final conversion. The user can then set these constants during the calibration procedure.

When the user installs the desired model inside the wind tunnel and fixes it on the dynamometer, the gravitational force causes the dynamometer to display a value proportional to the model's weight. In order to measure real values for lift (and if necessary, drag), the user can follow a zeroing procedure similar to that for the X and Y

sub-VIs. It is important, however, that the user set the slope to 1 before adjusting the offset for zero units of force with the wind tunnel off.

The dynamometer's high sensitivity makes it difficult to read a steady value for lift or drag when the laboratory is in progress. To filter out unwanted spikes, the lift and drag algorithms operate inside a *for loop*. Every 10 readings from the two parameters is averaged via a mean sub-VI whose output is then displayed on the front panel. The same outputs are also passed on a division module which divides the lift component by the drag component to display the valuable  $L/D$  (Figure 7.1).

### 7.3 Experimental/Validation Results

A variety of experiments can be performed using the CONSOLE.VI. Among these are

1. Zero-lift angle: The angle of attack  $\alpha$  at which an airfoil produces no lift is the zero-lift angle of attack ( $a_{L=0}$ ). Although symmetric airfoils have an  $a_{L=0}=0^\circ$ , asymmetric airfoils with positive camber, have an  $a_{L=0}<0^\circ$ . The NACA 4412 airfoil used to test this laboratory indicated an  $a_{L=0}$  at  $\alpha = -4^\circ$ .

2. Stall angle: The angle of attack  $\alpha$  at which the flow over the top surface of an airfoil separates, and a sharp decrease in lift is observed, is the stall angle. Immediately prior to reaching this condition, an airfoil experiences the maximum value of  $c_l$ , the  $c_{l,max}$ . The maximum coefficient measured for the NACA 4412 was

$$c_l = \frac{L}{\frac{1}{2} \cdot \rho_\infty \cdot V_\infty^2 \cdot c} = 1.167 \text{ @ } \alpha = 9^\circ \quad (7.2)$$

3. Drag models: One of the most important subjects of intermediate aerodynamics is the study of drag coefficients of various models with various surface textures. Drag is calculated using the following formula:

$$c_d = \frac{D}{\frac{1}{2} \cdot \rho_\infty \cdot V_\infty^2 \cdot c} \quad (7.3)$$

This formula was used to produce the results shown in Table 7.1.

**Table 7.1: Drag measurements for various models 4412 at 52 m/s**

<b>Model</b>	<b><math>c_d</math></b>
Rough sphere	0.00085
Smooth sphere	0.00092
Smooth disk	0.0029

## Chapter 8 : Pressure coefficients for NACA 4412

### 8.1 Theory

Experimenters often use data or theoretical solutions for one flow condition to gain insight into the flow field which exists for another flow condition. Wind tunnel data, where scale models are exposed to flow conditions that simulate the design-flight environment, are used to gain insight to describe the full-scale flow field at other flow conditions. It is most efficient to present a correlation in terms of dimensionless coefficients which depend only upon the configuration geometry and upon the angle of attack. One of these coefficients is the pressure coefficient:

$$C_p = \frac{p - p_\infty}{q_\infty} = \frac{p - p_\infty}{\frac{1}{2} \rho_\infty V_\infty^2} \quad (8.1)$$

The CP4412.VI uses the array from Section 3.1 to calculate pressure differences and convert them to coefficients of pressure for the NACA 4412 airfoil which has 9 upper and 5 lower pressure taps installed



## 8.2 VI Logic

The CONSOLE.VI uses the output from the PITOT.VI main sub-VI. The speed indicated by the pitot tube may optionally be used by the algorithm to calculate the pressure coefficient. Unfortunately, the dimensions of the test section are too small so when an airfoil is present, most practical areas for air-speed measurement within the traversing probe's travel are influenced either by the airfoil's wake, or the sidewalls of the wind tunnel. If the user desires to not use the real-time air-speed which is prone to errors, he can manually input the magnitude of velocity anticipated for the particular gap size. The selection between the two velocities (automatic or manual) is performed by a front-panel virtual switch.

The relatively large array of pressure transducers in a confined area made routing of pressure tubes problematic. The layout chosen allows for the transducers to measure the differential pressure between each pressure tap on the airfoil and the room in which the wind tunnel is located. To compensate for the reference pressure difference, one transducer is used to measure the difference between the room and the wind tunnel static pressure. The value of this last transducer is subtracted from each pressure tap's value resulting in the pressure difference between each pressure tap and the wind tunnel freestream (Figure 8.1):

Pressure transducers measure :

$$\Delta P_{1-8\&10-14} = p_{room} - p_{spot} \quad (8.2)$$

$$\Delta P_9 = p_{room} - p_{spot9} \quad (8.3)$$

Lets assume measurement at spot 2 :

$$\Delta P_2 = p_{room} - p_{spot2} \quad (8.4)$$

$$p_{\infty} = p_{spot9} \quad (8.5)$$

So, from (8.4) and (8.5),

$$\begin{aligned} \Delta P_2 - \Delta P_9 &= \\ &= (p_{room} - p_{spot2}) - (p_{room} - p_{spot9}) = \\ &= p_{room} - p_{spot2} - p_{room} + p_{spot9} = \\ &= p_{spot9} - p_{spot2} \Rightarrow \\ &\Rightarrow \Delta P_2 - \Delta P_9 = p - p_{\infty} \end{aligned} \quad (8.6)$$

The clustered installation of the pressure transducers results in slight discrepancies of output values at rest. Instead of showing zero pressure difference when the wind tunnel is not running, most of the sensors are slightly offset. The offset values were determined during calibration and were used on each unit to set the reference point. Each transducer's offset is subtracted from its respective output and divided by the freestream dynamic pressure.

The resulting value from each set of calculations is displayed both numerically and graphically on the front panel of the VI. The graphical representation is designed to simulate the look of a manometer array (Figures 8.2, 8.3).

### 8.3 Experimental/validation Results

**Table 8.1: Validation results**

<b>Position</b>	<b>NASA experimental data [7]</b>	<b>LabVIEW experimental data</b>
0 upper	-0.05	-0.08
1 upper	-0.10	-0.12
2 upper	-1.74	-1.74
3 upper	-1.34	-1.33
4 upper	-1.00	-1.04
5 upper	-0.92	-0.93
6 upper	-0.48	-0.44
7 upper	-0.42	-0.38
8 upper	-0.40	-0.43
10 lower	0.78	0.73
11 lower	0.62	0.59
12 lower	0.37	0.33
13 lower	0.17	0.15
14 lower	0.12	0.12

## Chapter 9 : Sub2D

### 9.1 Introduction

SoftwAeronautics' Sub2D subsonic aerodynamics softer for Windows is one additional tool that can assist in studying steady flows which could in turn be verified or compared to experimental data acquired with the LabVIEW test environment. While Sub2D is a versatile program, for the purposes of this discussion, only a few of its features were used to illustrate its complimentary role as an aerodynamics learning tool.

### 9.2 Features

Sub2D is a powerful interactive tool for analysis and visualization of 2-D steady subsonic aerodynamics and runs under the Microsoft Windows environment [9]. Sub2D can simulate the flow of fluids around one or more bodies with interactive control over Mach number, Reynolds number, angle of attack, boundary layer transition, and boundary layer separation.

The built-in model generator can be used to instantly create models of circular cylinders, ellipses, rectangles, and a wide variety of airfoils. The displayed data can be selected to include surface pressures, streamlines, source and vortex strengths, forces and moments, boundary layers, stagnation points, transition points, separation points, and color-shaded flowfield pressures. In addition, plots of  $C_l$  vs  $\alpha$ ,  $C_z$  vs  $\alpha$ ,  $C_m$  vs  $\alpha$ ,  $C_z$  vs  $C_p$ ,  $C_m$  vs  $C_z$ ,

and  $C_p$  vs  $\frac{x}{c}$  can be created. Local flow properties can be instantly revealed by simply pointing with a mouse, including position, velocity vector, Mach number, and pressure coefficient. The images and data created using Sub2D can be easily shared with other applications, including word processors and spreadsheets, through the Windows clipboard.

Students will find Sub2D's visualizations of aerodynamics data to be an exciting supplement to the abstract equations found in textbooks. Airfoils pitch up and down in response to commanded angle of attack. Streamlines show the paths taken by fluid particles to avoid objects immersed in the flow. Colors reveal the intricate swirling patterns of pressures in the flowfield. Surface pressures are seen pushing and pulling on bodies to create lift and drag. Boundary layers visibly grow, transition, and separate. Source and vortex panel strengths are seen to vary in magnitude and direction to continuously enforce boundary conditions in response to changes in the freestream. Sub2D is ideal for use in class projects and theses because of the ease with which high-quality graphics can be created and incorporated in documents.

Additionally, practicing aeronautical engineers will find Sub2D to be an indispensable tool for preliminary analysis and visualization of 2-D steady subsonic flow problems. It can be used to analyze viscous or inviscid flows with or without compressibility. To achieve reasonable accuracy and acceptable or inviscid flow performance on personal computers, Sub2D employs theoretical methods for compressible inviscid flow solutions and semi-empirical methods to account for viscous effects. Linear potential theory, employing source and vortex panels, is used to calculate inviscid flowfields. Compressibility effects can be calculated using the Prandtl-Glauert correction, the Karman-Tsien correction, or by

solving the Prandtl-Glauert equation. For viscous analyses, boundary layer growth is calculated using Thwaites' integral method for laminar boundary layers and Head's integral method for turbulent boundary layers. Boundary layer transition and separation are predicted using semi-empirical methods.

The accuracy of Sub2D's flowfield calculations depends upon the complexity of the analysis. For incompressible, inviscid analyses, Sub2D's, calculated flowfields, rapidly approach exact solutions as the number of panels is increased. For compressible analyses, the accuracy of the Sub2D calculations depends on the selected compressibility correction method and degrades as the Mach number increases. Once the critical Mach number is reached, the flow is no longer purely subsonic and the basic assumptions of Sub2D's methods are violated. Viscous flowfields are immensely more complicated than inviscid flowfields. Even modern super computers are taxed by the task of calculating simple viscous flowfields using the latest finite-difference techniques. Sub2D incorporates a simpler hybrid inviscid/viscous method to permit solutions on personal computers. Viscous flowfield calculations with Sub2D are therefore less accurate than inviscid calculations. Accuracy decreases when significant flow separation occurs, such as for airfoils near the stall angle of attack. However, Sub2D's calculations of airfoil minimum skin friction drag are in general quite good for Reynolds numbers from  $10^6$  to  $10^7$ . Estimation of form drag is Sub2D's weakest capability, owing to the great difficulty in determining the effects of the boundary layer on flowfield pressures. User control over key parameters allows correlation of viscous flow calculations to available experimental data.

### **9.3 Integration with LabVIEW**

Sub2D can simulate laboratory conditions using theoretical models and algorithms. Data collected and plots created with Sub2D can be compared with data and plots from LabVIEW. This can illustrate the differences between experimental and theoretical environments, as well as point out deficiencies in either setup. Comparing the two, students familiarize themselves with the research methods normally used to create and validate an aerodynamic model. They can also decipher problem areas with either environment allowing them to make improvements when needed.

Sub2D's capability to graphically illustrate the differences between viscous and inviscid flows allows students to get a good feel for the discrepancies in the results acquired using ideal conditions versus making good assumptions. Finally, Sub2D's ability to simulate many four, and five digit NACA airfoils allows students to experiment with such a variety of airfoils and environments that would otherwise be to perform experimentally.

### **9.4 Results**

Figures 9.1, 9.2, 9.3, and 9.4 illustrate the quality graphs that Sub2D can produce. Results from these graphs can be verified or compared against theoretical and experimental data.

## **Chapter 10 : Conclusions and Recommendations**

### **10.1 Conclusions**

Computer-controlled data acquisition systems are not limited to large laboratory applications. They can also be used in developing real-time monitoring undergraduate laboratories. LabVIEW is one such system and was used in conjunction with computer hardware and sensors in order to create an automated wind tunnel monitoring setup.

The algorithms used were within acceptable margins of error when compared with sophisticated large scale data acquisition systems.

The overall system provided quick, repeatable, and accurate information bound only by the sensors' physical limitations and sensitivities. Results obtained from the experiments devised compared favorably with theoretical data from the Sub2D software for aerodynamics.

### **10.2 Recommendations**

1. Some of the instability of the current LabVIEW VIs is caused by the lack of sophisticated filtering functions in the algorithms. Ground inefficiencies in the instrumentation and RF disturbances tend to interfere with electrical signals causing unsteady behavior. Filtering adds significant CPU loads, which in turn demand a fast



computer. It is recommended that before updating the algorithms the system be installed on a Pentium-class computer.

2. The front panels used throughout the laboratories and their VIs are limited by the size of the screen used (15" total, 12.5" visible). Larger screens permit the creation of a better, less cluttered interface, which in turn allows easier monitoring of functions and sensors.
3. The version of LabVIEW for this series of laboratory exercises is already outdated and has been replaced by version 4.0.1 in National Instruments' product line. The newer version of LabVIEW offers advanced DAQ VIs and File I/O utilities that would enhance the usability of the software and allow students to collect data and, process, and present data using appropriate statistical analysis tools.
4. The pressure transducers used in the current setup have a very wide range compared to the typical values expected. Omega and Microswitch offer a variety of pressure transducers which can easily replace the current ones. The hardware installation does not present a problem as all sensors are mounted with replaceable plugs and are not bonded on the container box. Sensors that limit their range to  $\pm 1$  psi or  $\pm 2.5$  psi would be more appropriate as they would provide a wider resolution per psi.
5. LabVIEW is capable of not only processing input signals but also of controlling external devices with appropriate input connections. The 12" ELD wind tunnel requires manual operation of the gap downstream from the test section, in order to control the air velocity. ELD offers an upgrade kit through which eliminates the need to increase and decrease the gap. The kit consists of a new 10 hp motor with a variable frequency inverter to regulate the fan-shaft RPM. A remote sensor can be mounted near the test section and the inverter can be operated remotely via an RS-232 connector or via a servo controlled by LabVIEW. Additionally, a fusible disconnect can serve as primary protection for the inverter/motor combination. Both the inverter and the disconnect can

be mounted to the existing wind tunnel frame and the fan can be positioned in a fixed location relative to the wind tunnel ducts.

6. A more sophisticated setup may also include a step-motor attachment to control the angle of attack for airfoils inside the test section. Although its fixed mounting position will be incompatible with the dynamometer's required degree of freedom, it can assist in running complete tests on airfoils with pressure taps, as in the NACA 4412 case. LabVIEW algorithms can complete full tests for zero angle of attack, stall angle, etc. in a matter of minutes, thus providing quick and detailed experimental data.

## References

- [1] Engineering Laboratory Design: *Instruction Manual Wind Tunnel Instrumentation System*, Engineering Laboratory Design, Inc., Lake City, MN., 1989
- [2] National Instruments: *LabVIEW Tutorial and Manuals*, National Instruments Corp., Austin, TX., 1994
- [3] National Instruments: *<http://www.natinst.com/products>*, National Instruments Corp., World Wide Web, 1996
- [4] Anderson, J.D., *Introduction to Flight, 3rd edition*, McGraw Hill, Inc. New York, NY., 1989
- [5] Anderson, J.D., *Fundamentals of Aerodynamics, 2nd edition*, McGraw Hill, Inc. New York, NY., 1991
- [6] Bertin, J.J., *Aerodynamics for Engineers, 2nd edition*, Prentice Hall, Englewood Cliffs, NJ., 1989
- [7] Pinkerton, R.M., *Calculated and Measured Pressure Distributions of the Midspan Section of the NACA 4412 Airfoil, Report 563*, NACA, 1936
- [8] SoftwAeronautics: *Sub2D for Windows User's Guide, version 1.0*, SoftwAeronautics, Inc., Kennesaw, XX., 1995

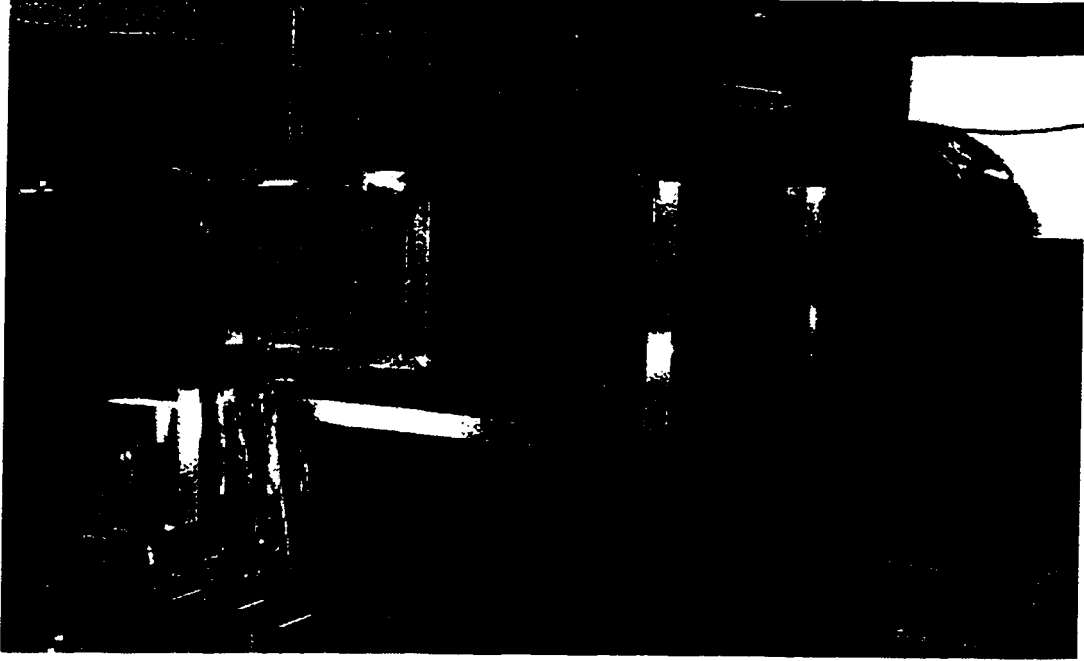


**Fig. 2.1: 12" Wind tunnel**

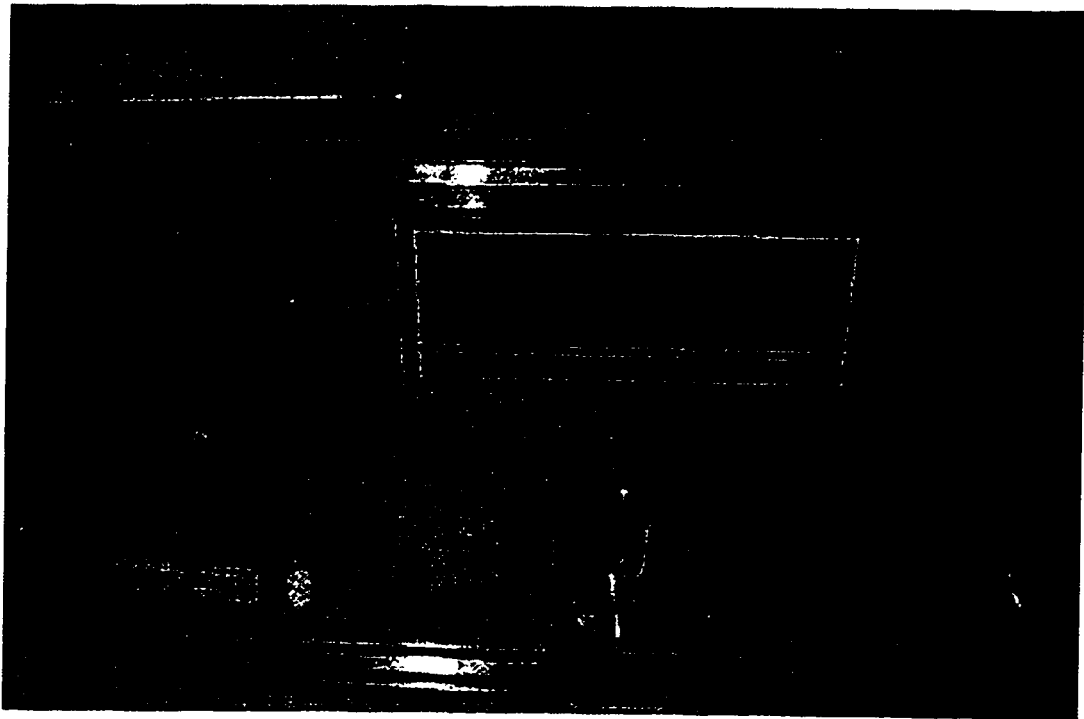


**Fig. 2.2: ELD Meter Cabinet**

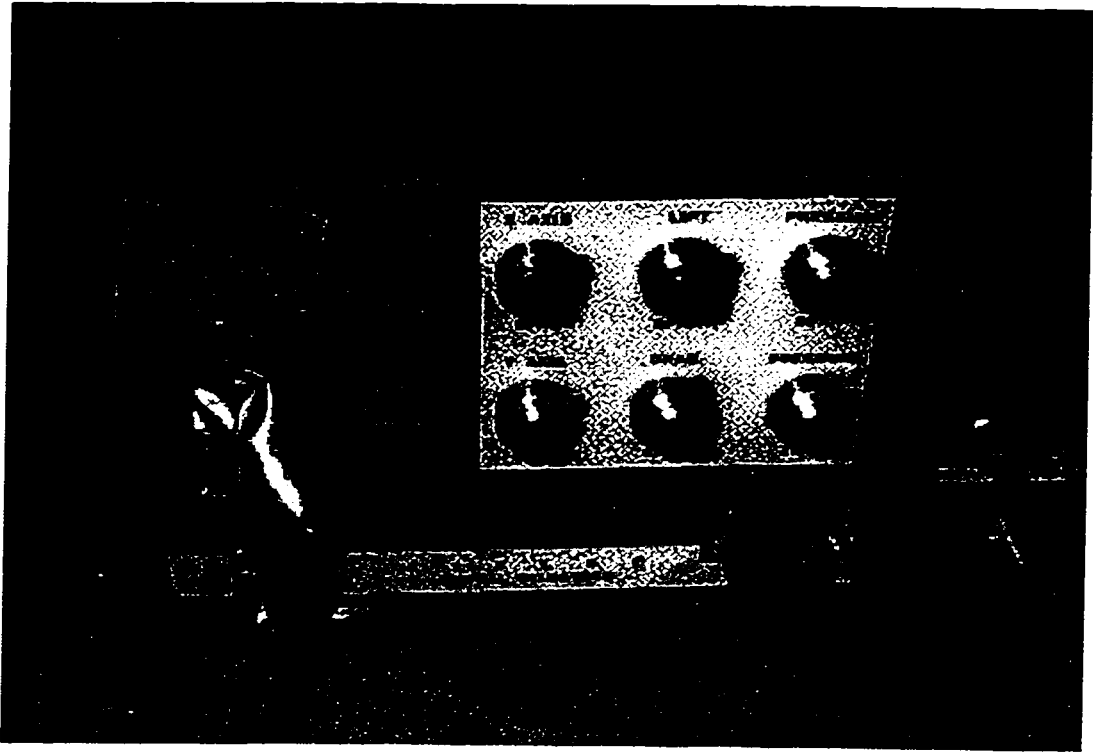


**Fig. 2.3 : Meter cabinet calibration controls**

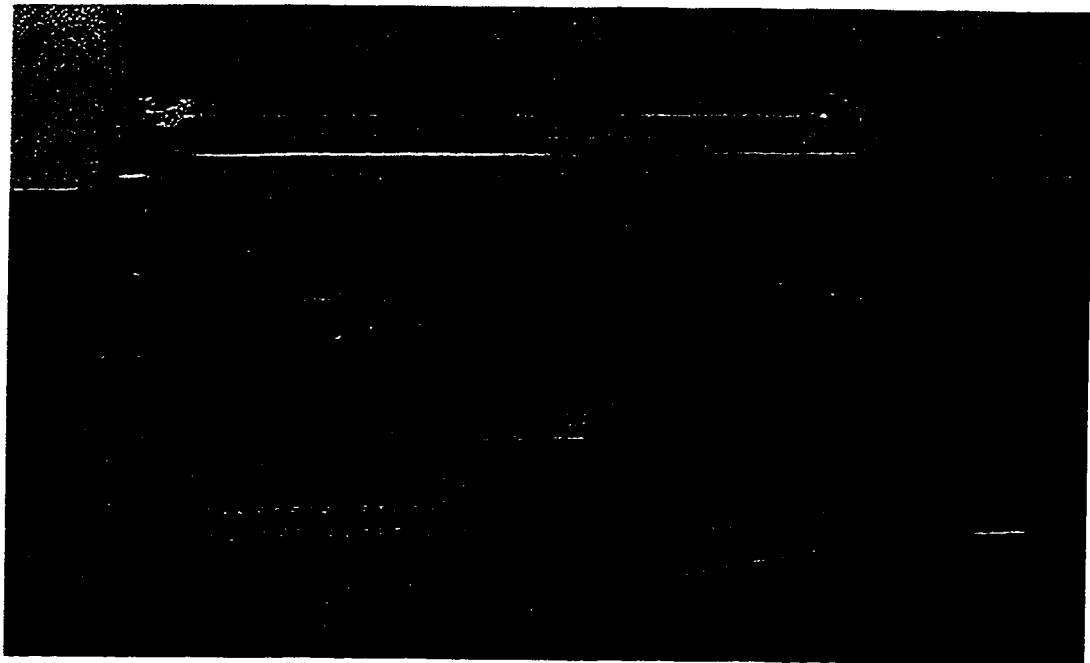


**Fig. 2.4: Test section with NACA 4412 and dynamometer**

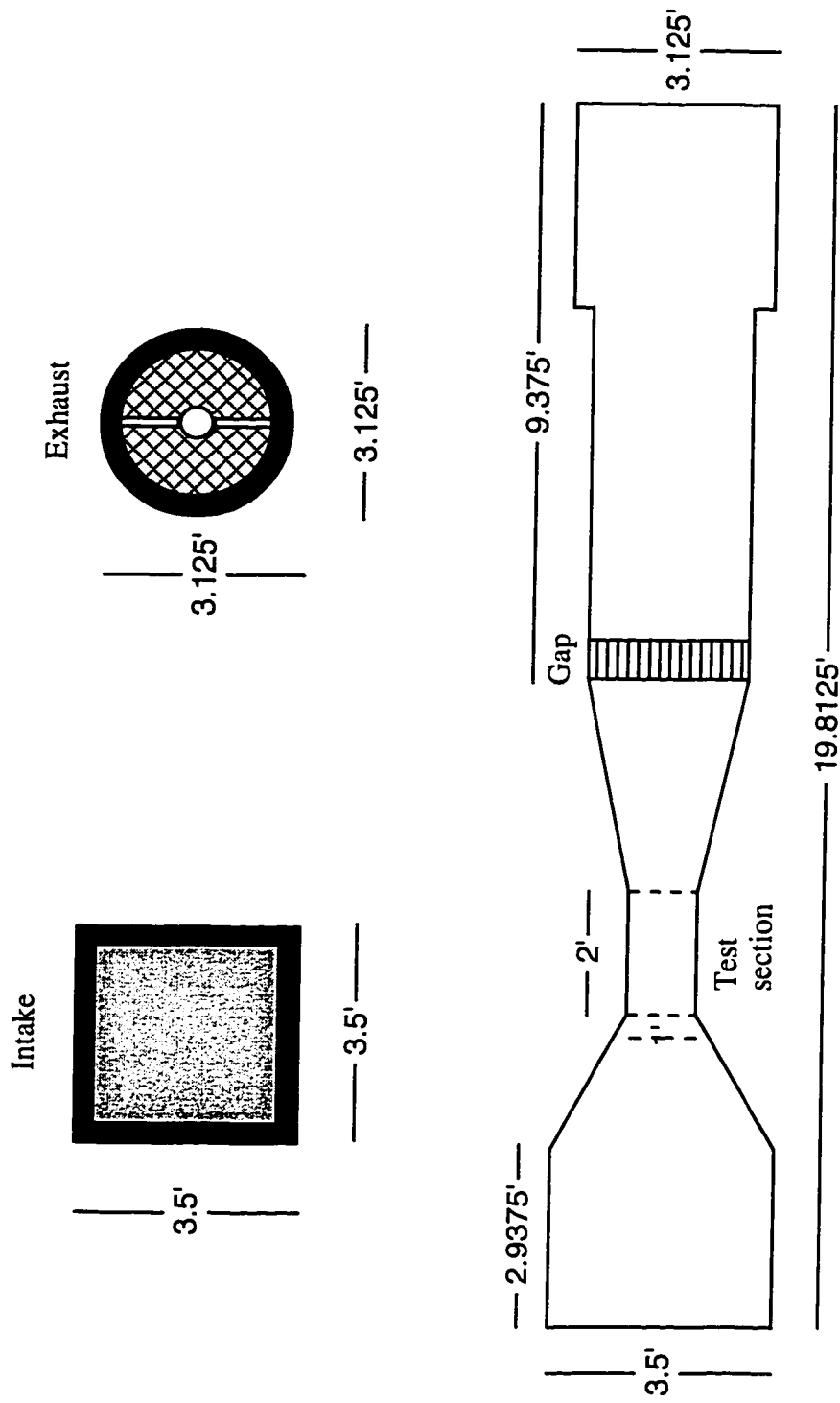


**Fig. 2.5: Wind Tunnel Dimensions**

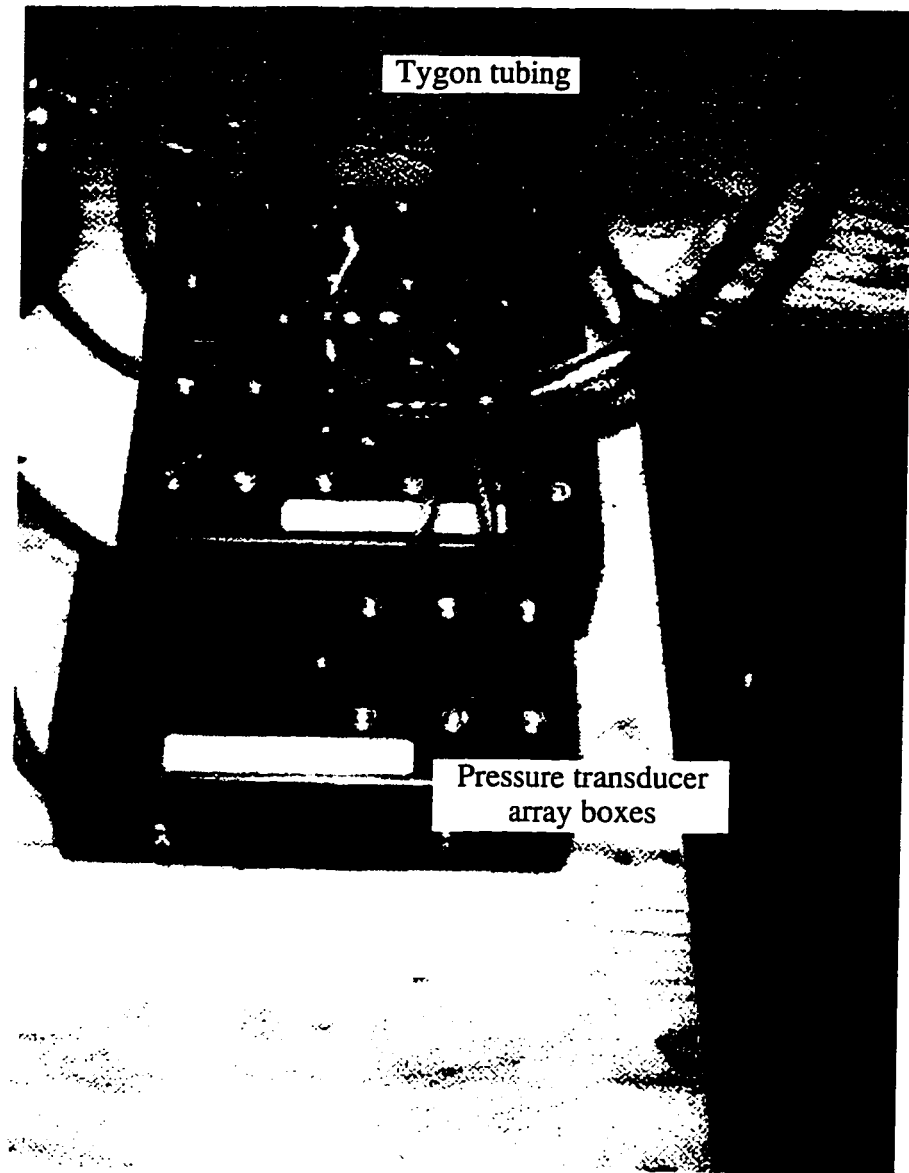


**Fig. 3.1: Pressure transducer array**

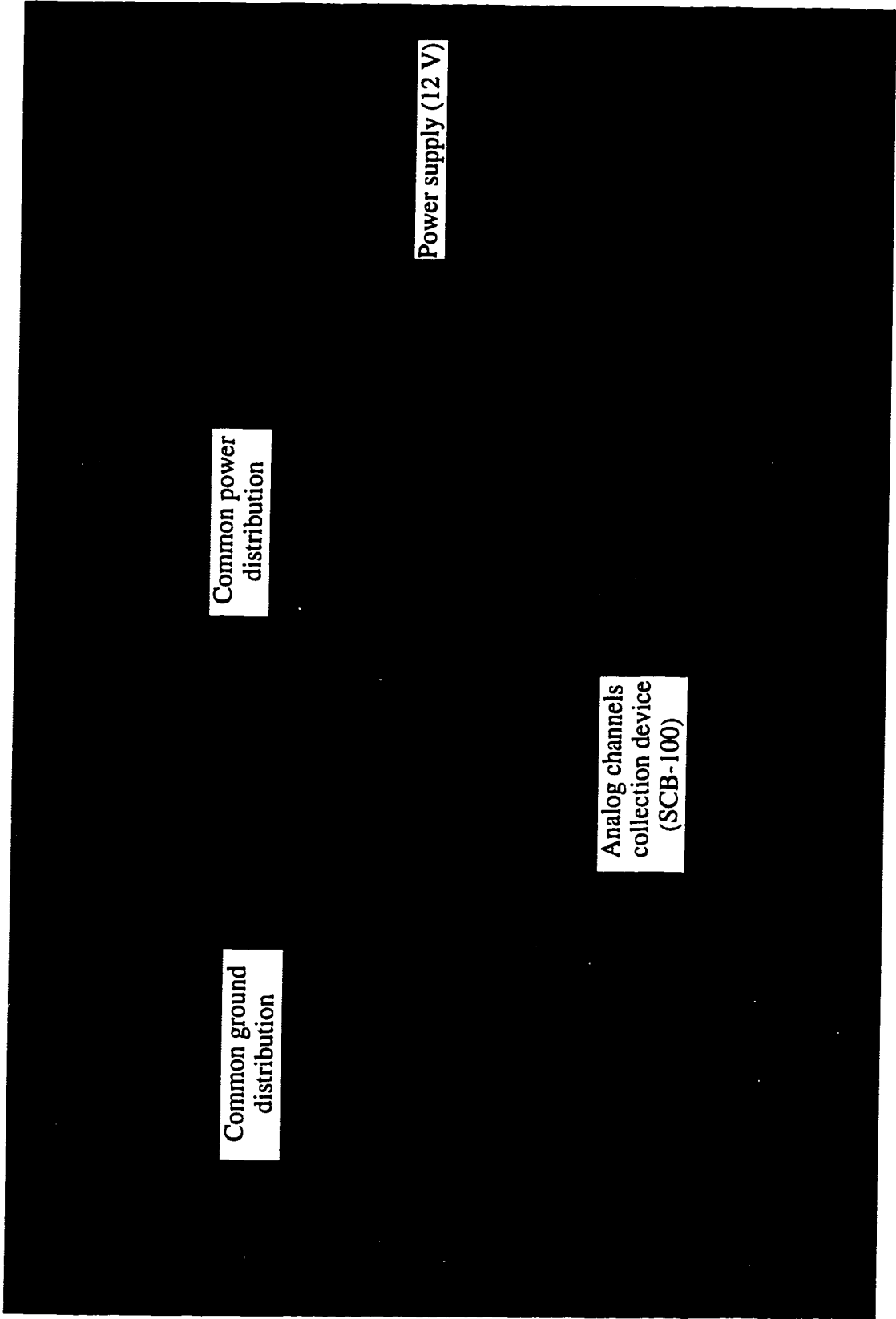


**Fig. 3.2: Power and ground distribution, and power supply**



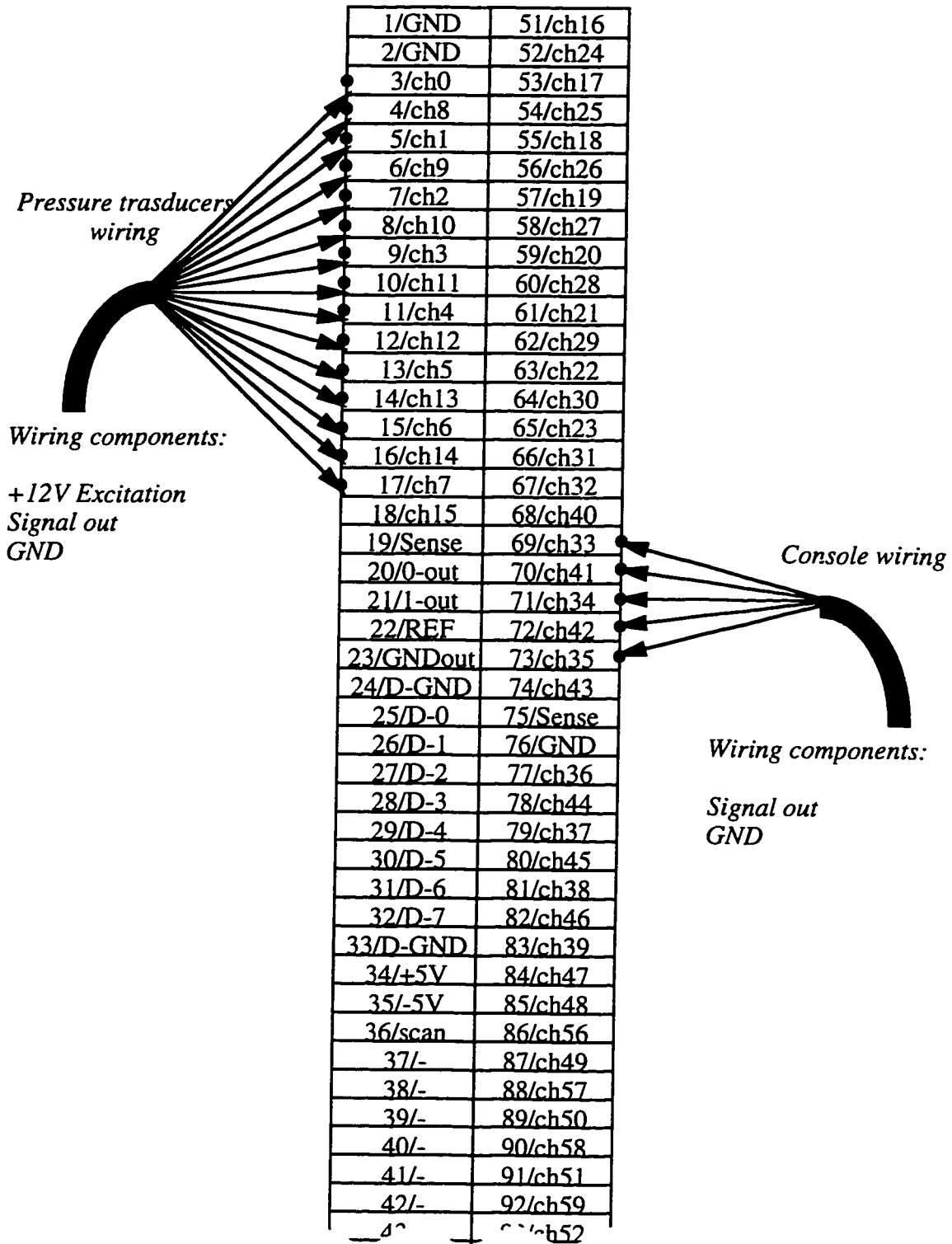


**Fig. 3.3: SCB-100 wiring diagram**

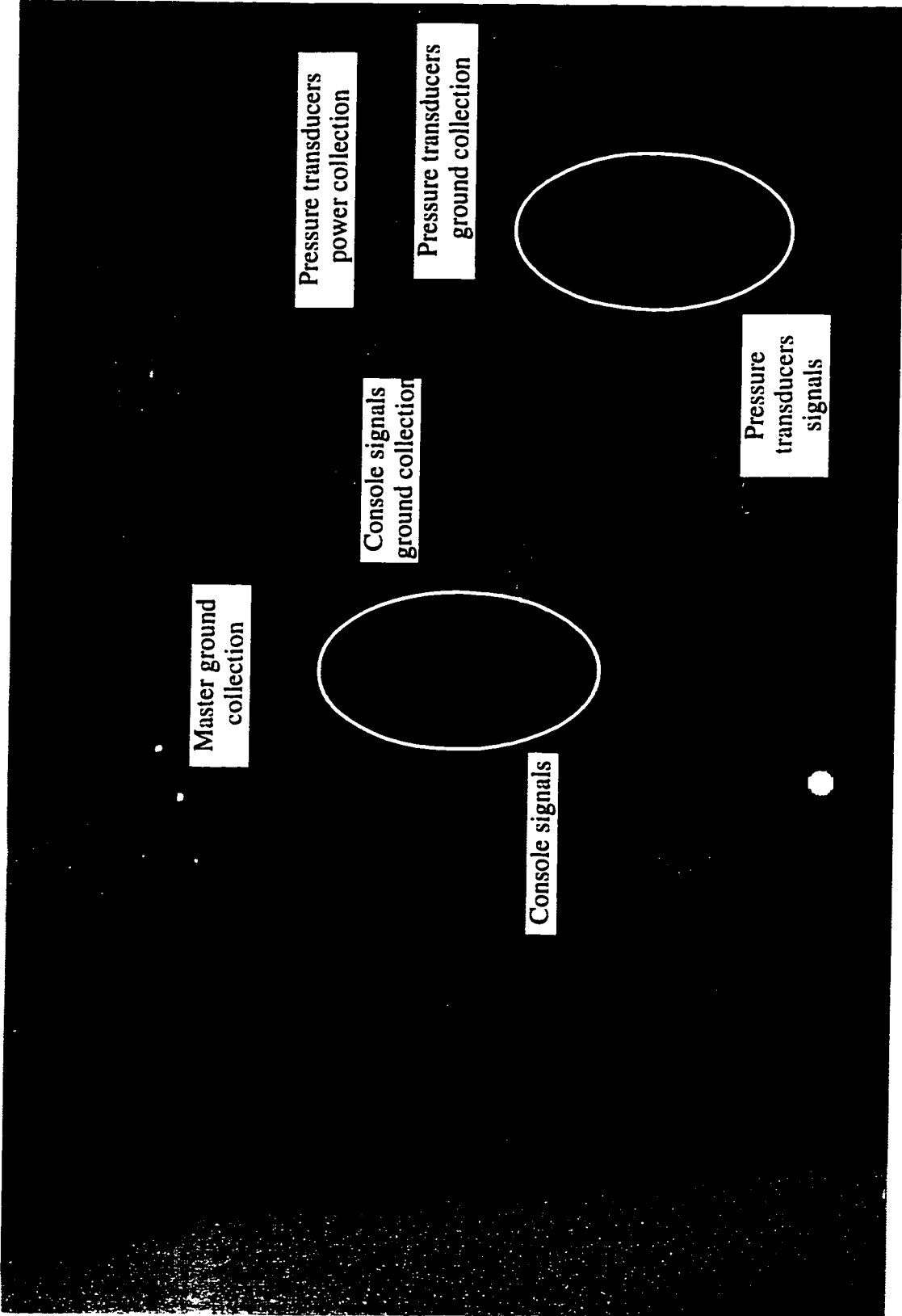


**Fig. 3.4: SCB-100 layout**

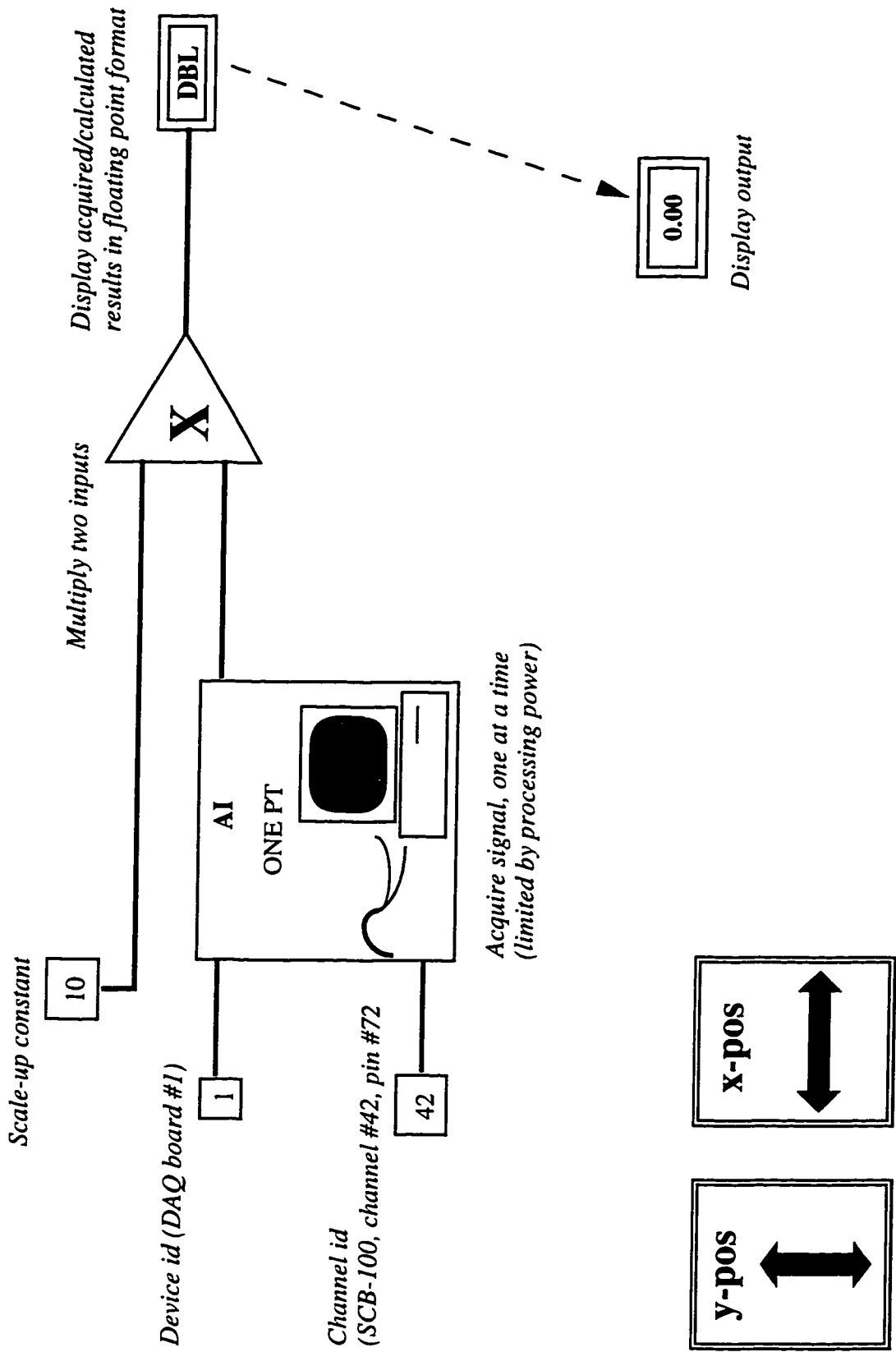


Fig. 5.1: X-POS.VI - x-position subroutine

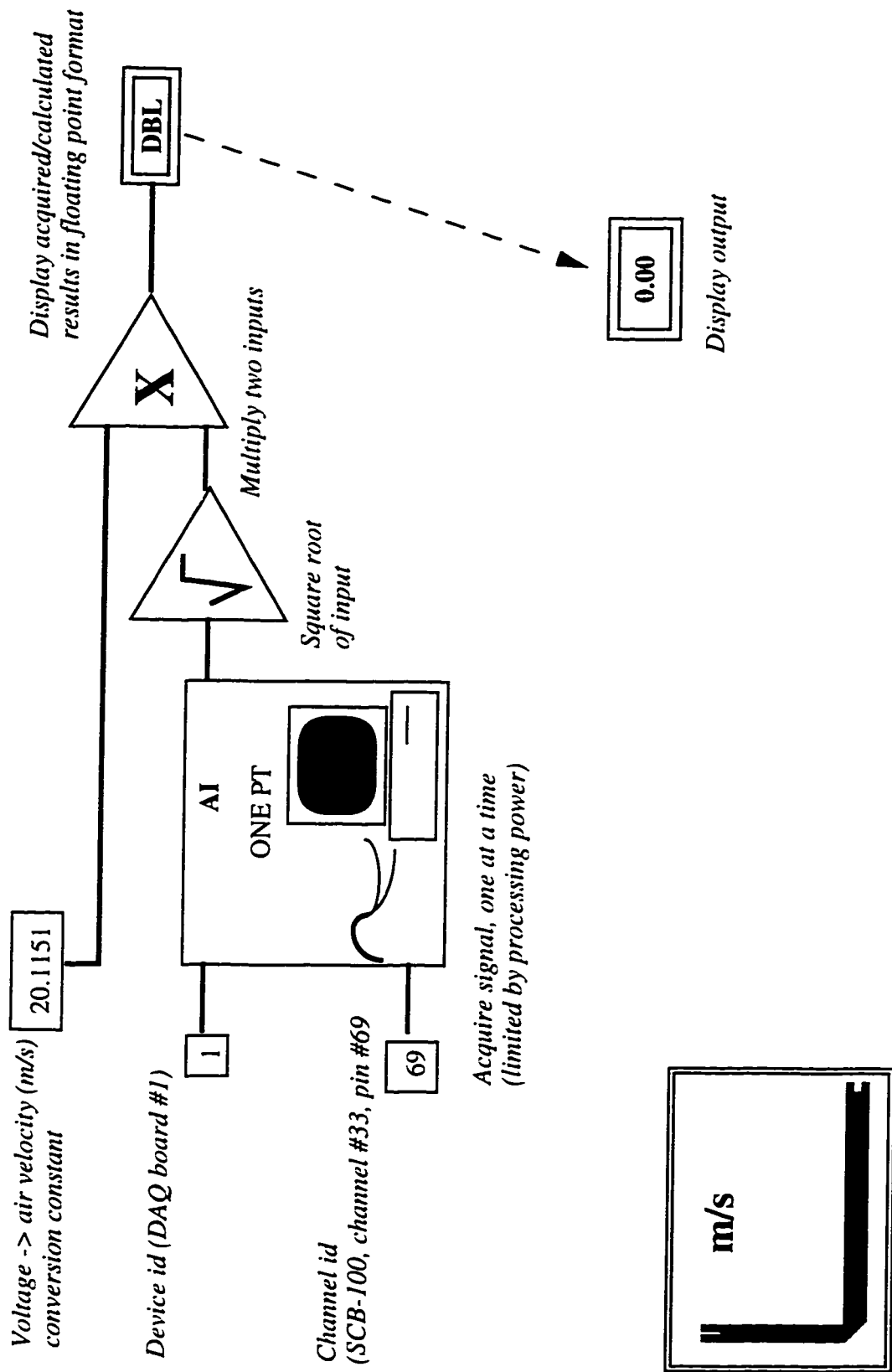
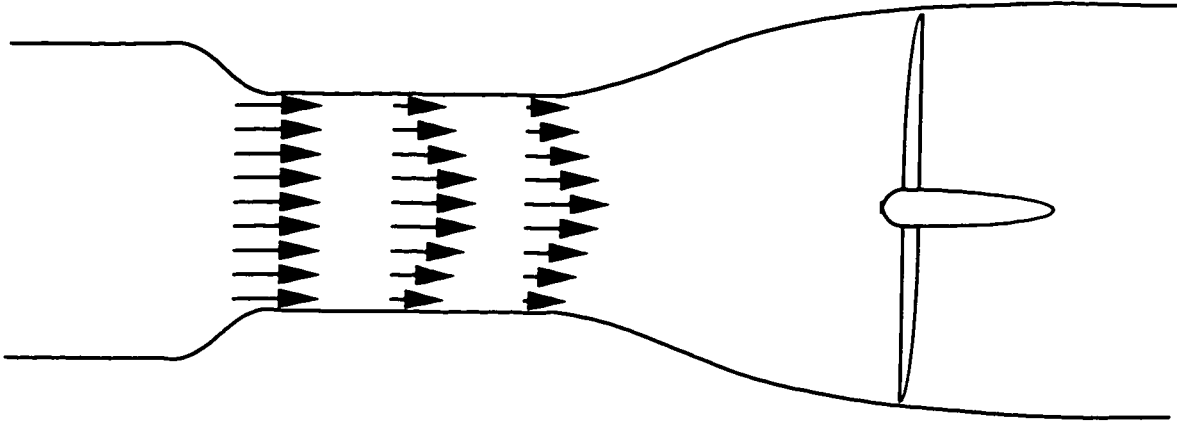
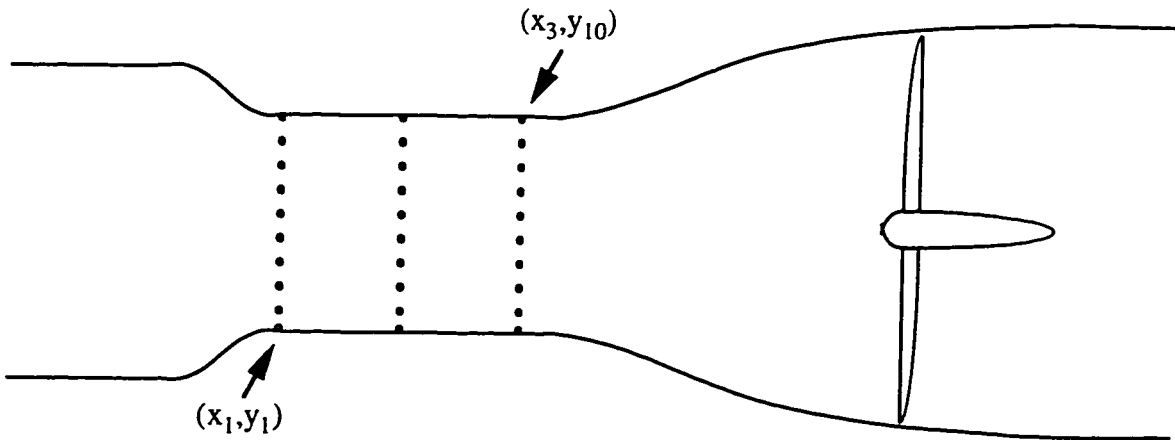


Fig. 5.2: PITOT.VI - Pitot tube subroutine



**Fig. 6.1: Exaggerated flow behavior inside a wind tunnel's test section**



**Fig. 6.2: Flow quality measurement matrix**

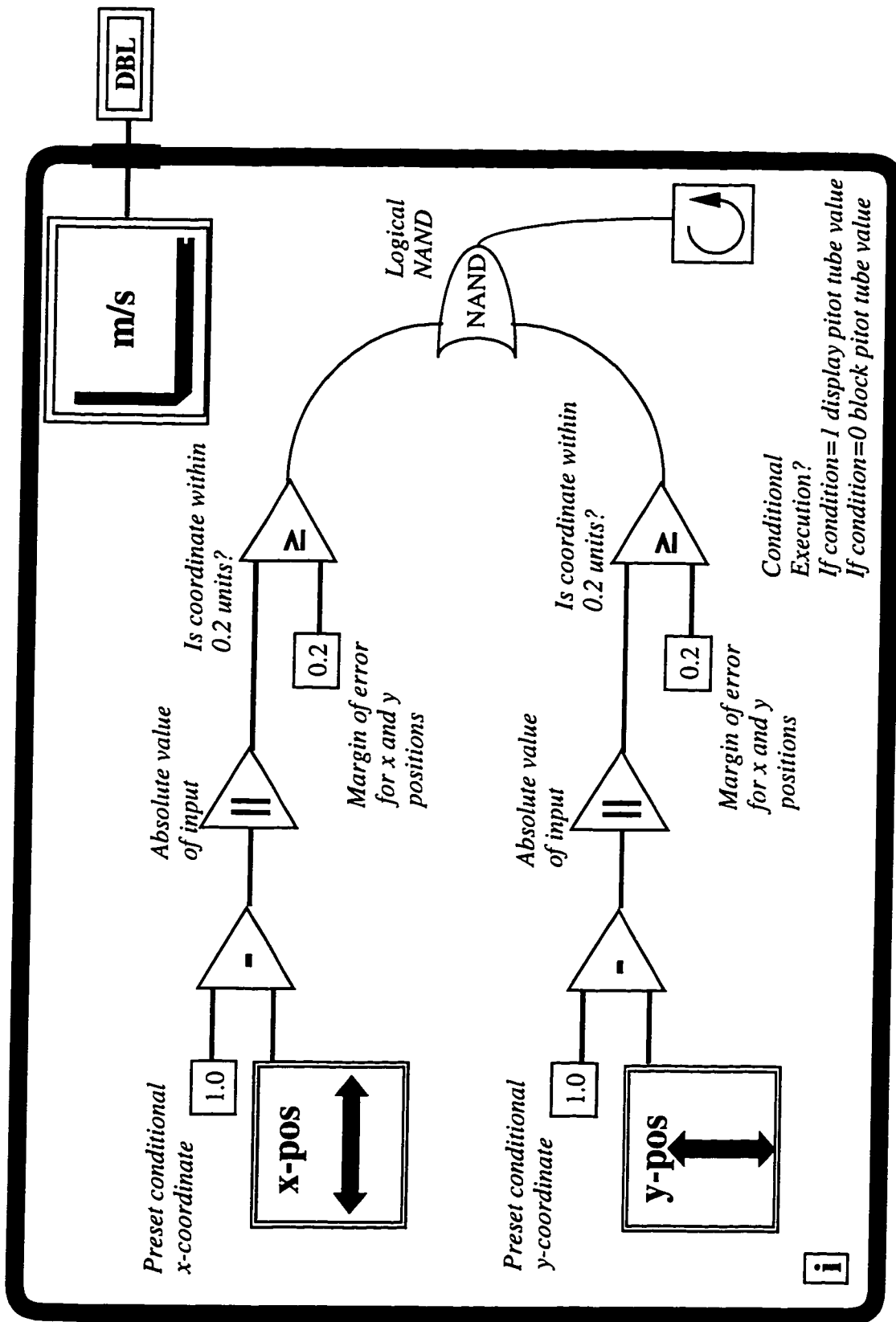
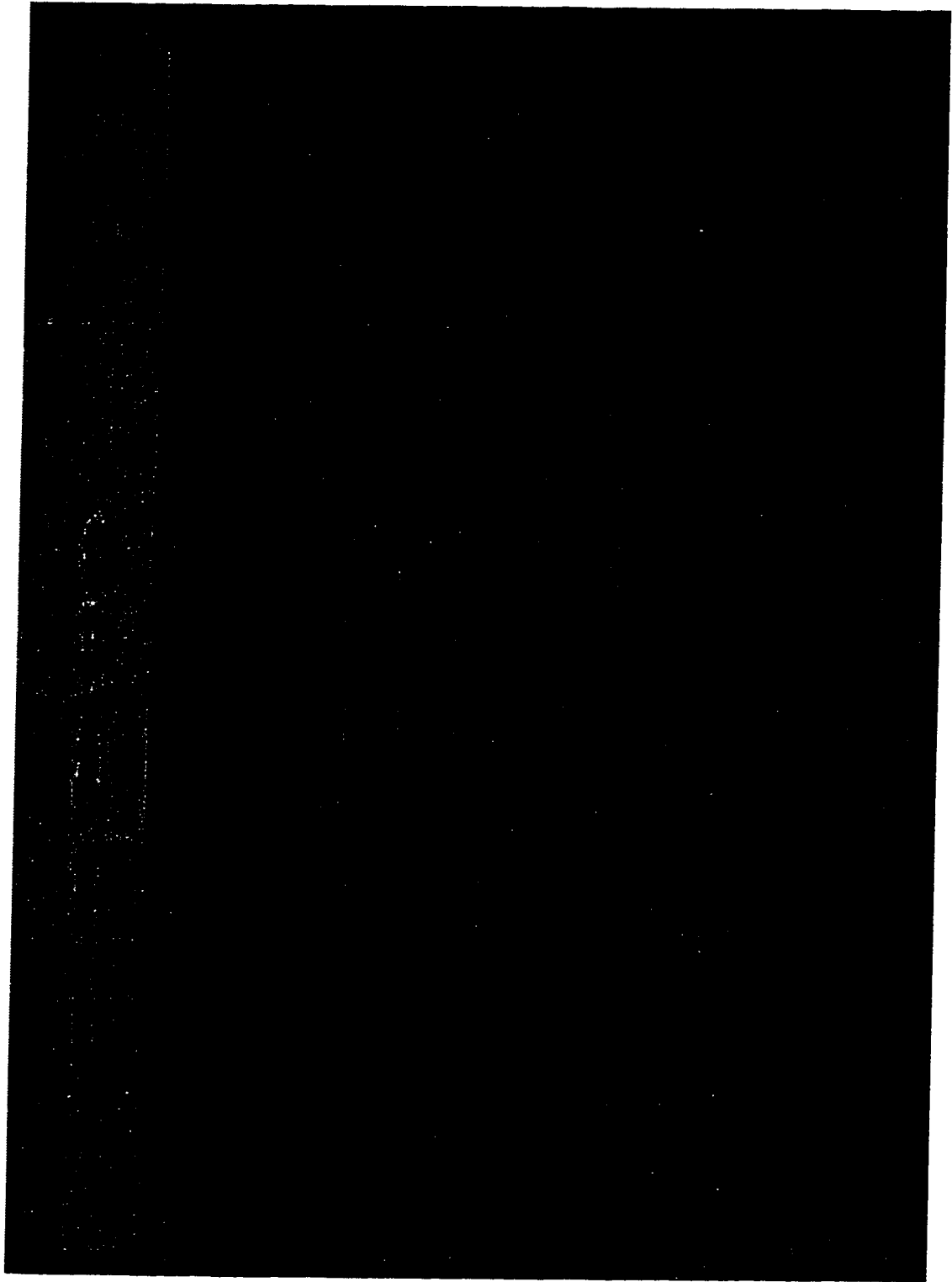
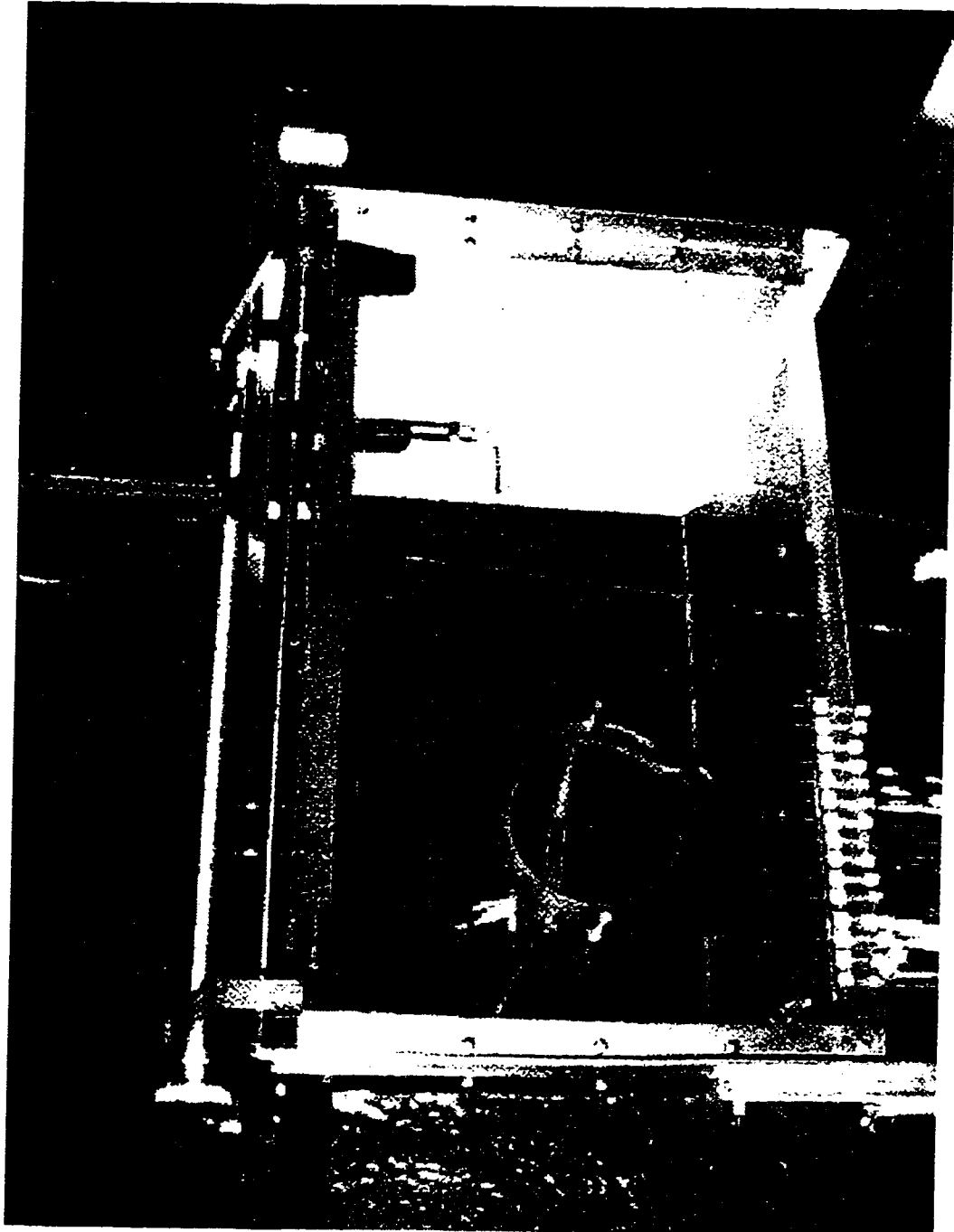


Fig. 6.3: X,Y,VI - Fixed position velocity measurement

While loop



**Fig. 6.4: Air velocity matrix - 30 points**



**Fig. 6.5: Wake drag setup**



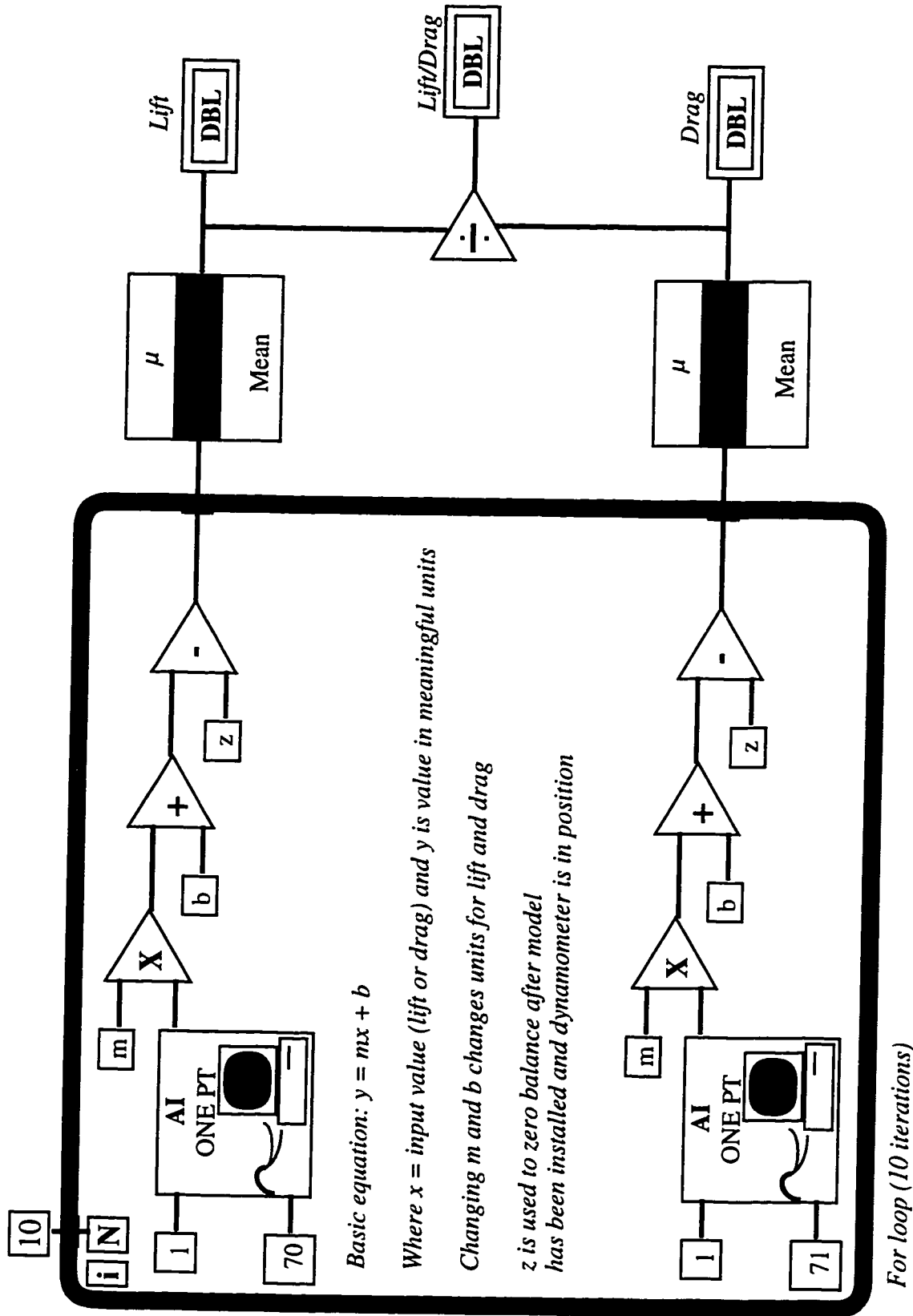


Fig. 7.1: CONSOLE.VI - Lift & Drag components

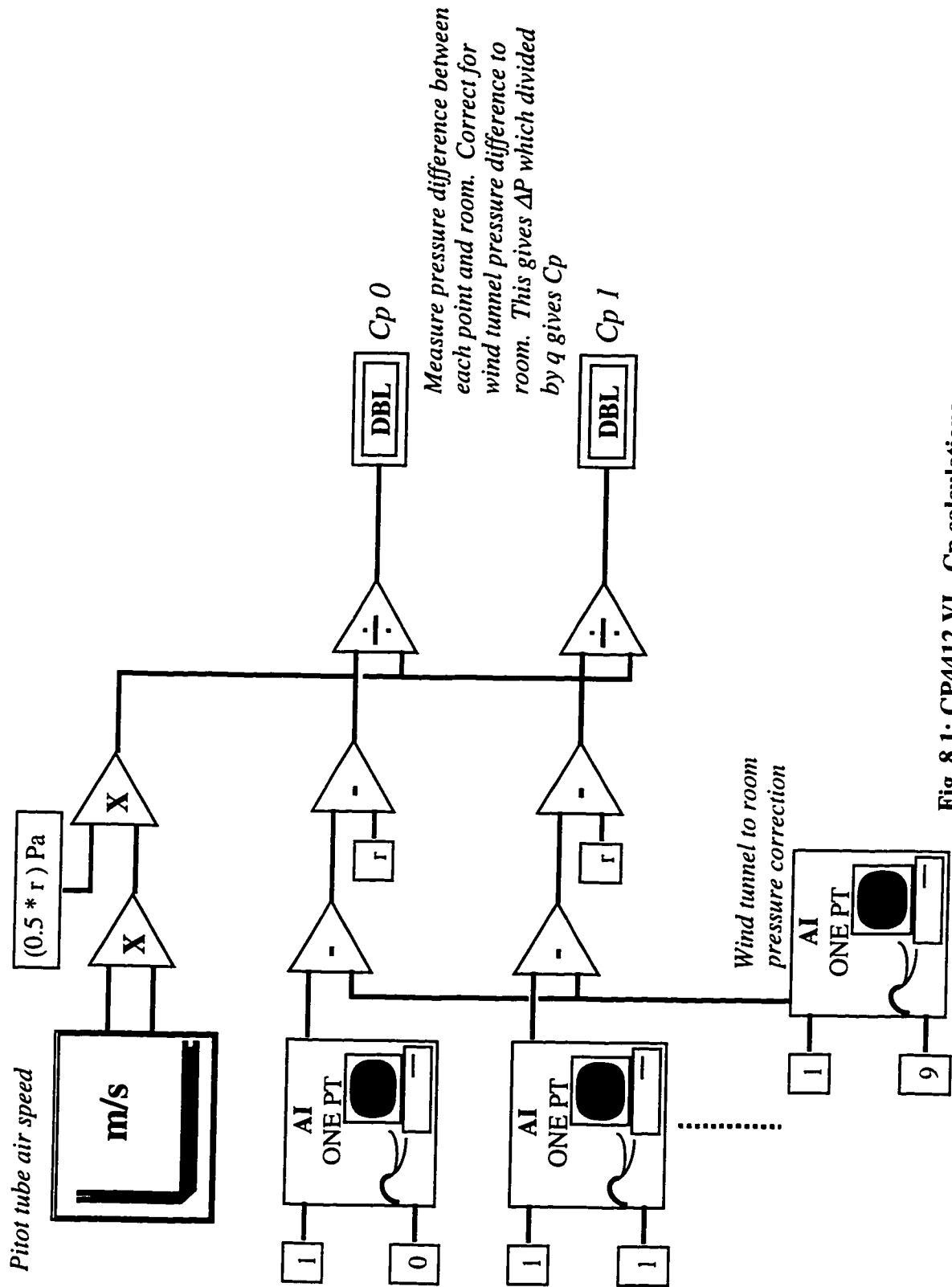
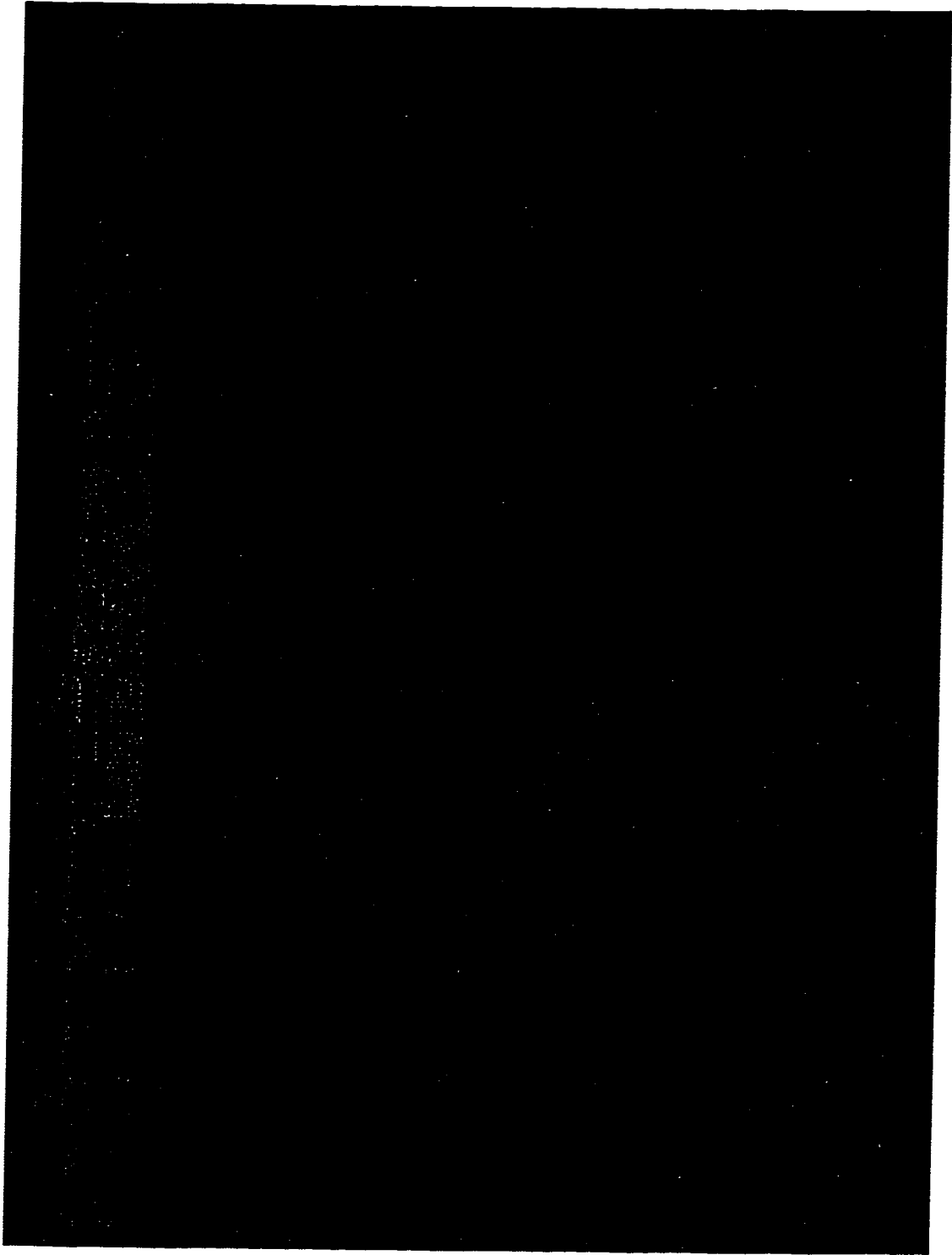
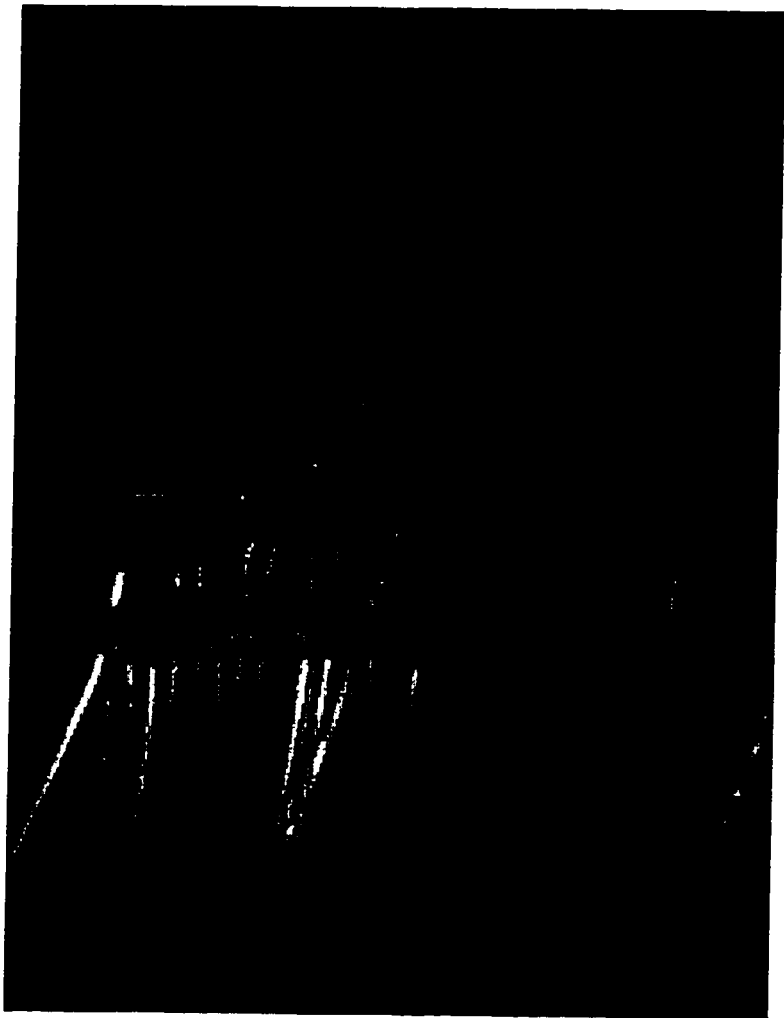


Fig. 8.1: CP4412.VI - Cp calculations



**Fig. 8.2: CP4412.VI at 0m/s**



**Fig. 8.3: Test section with NACA 4412 and tubing**

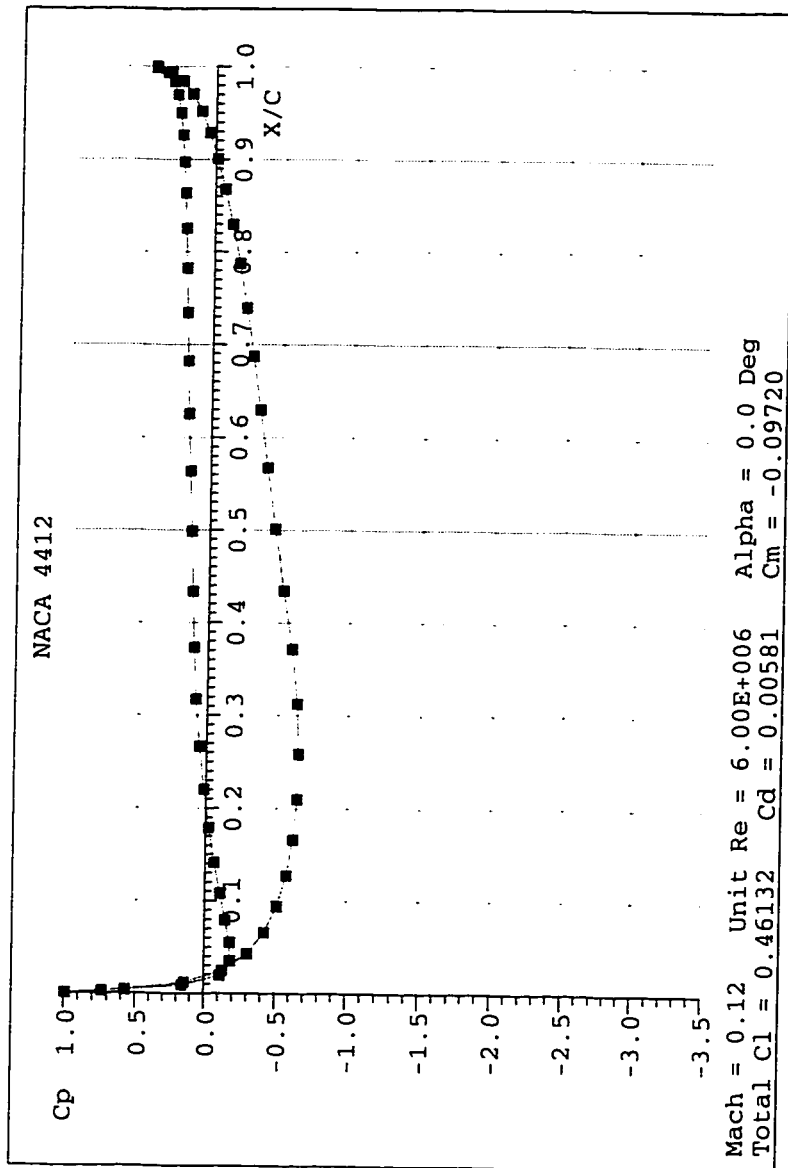


**Fig. 9.1: Sub2D Output -  $C_p$  distribution at  $M = 0.12$ ,  $\alpha = 0^\circ$**

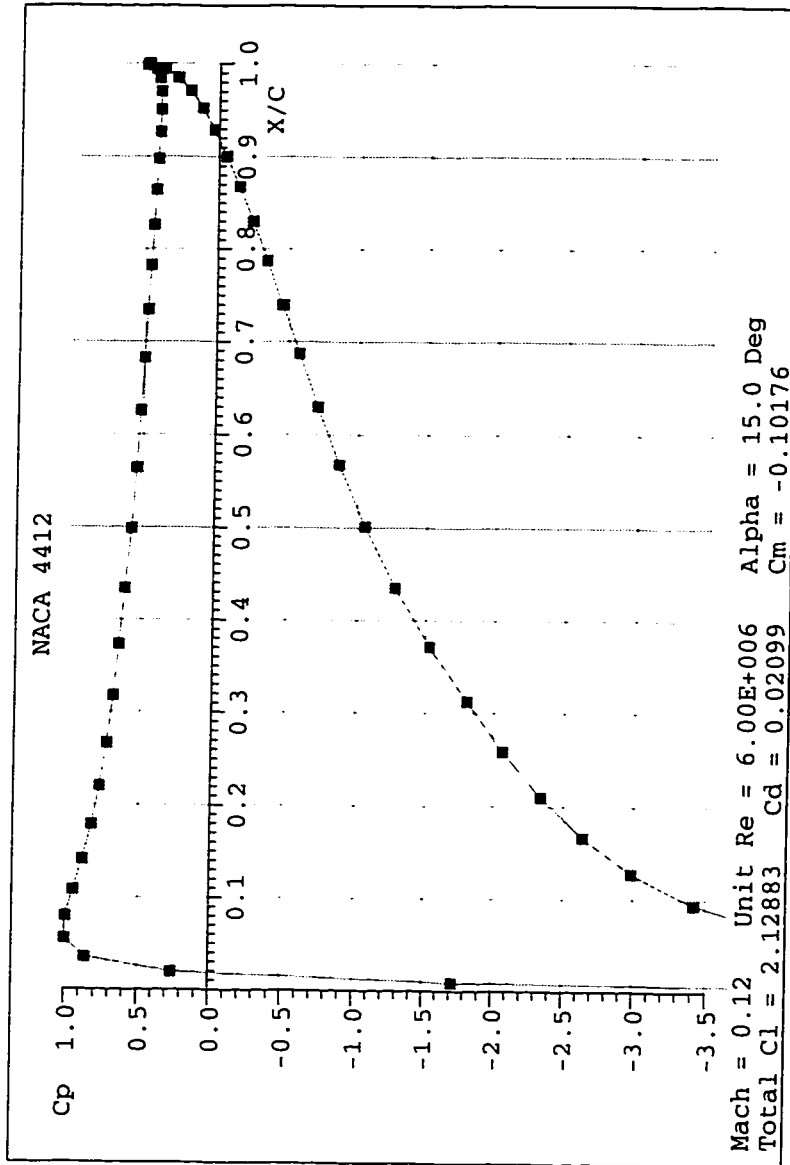


**Fig. 9.2 : Sub2D Output - Cp distribution at M = 0.12,  $\alpha = 15^\circ$**

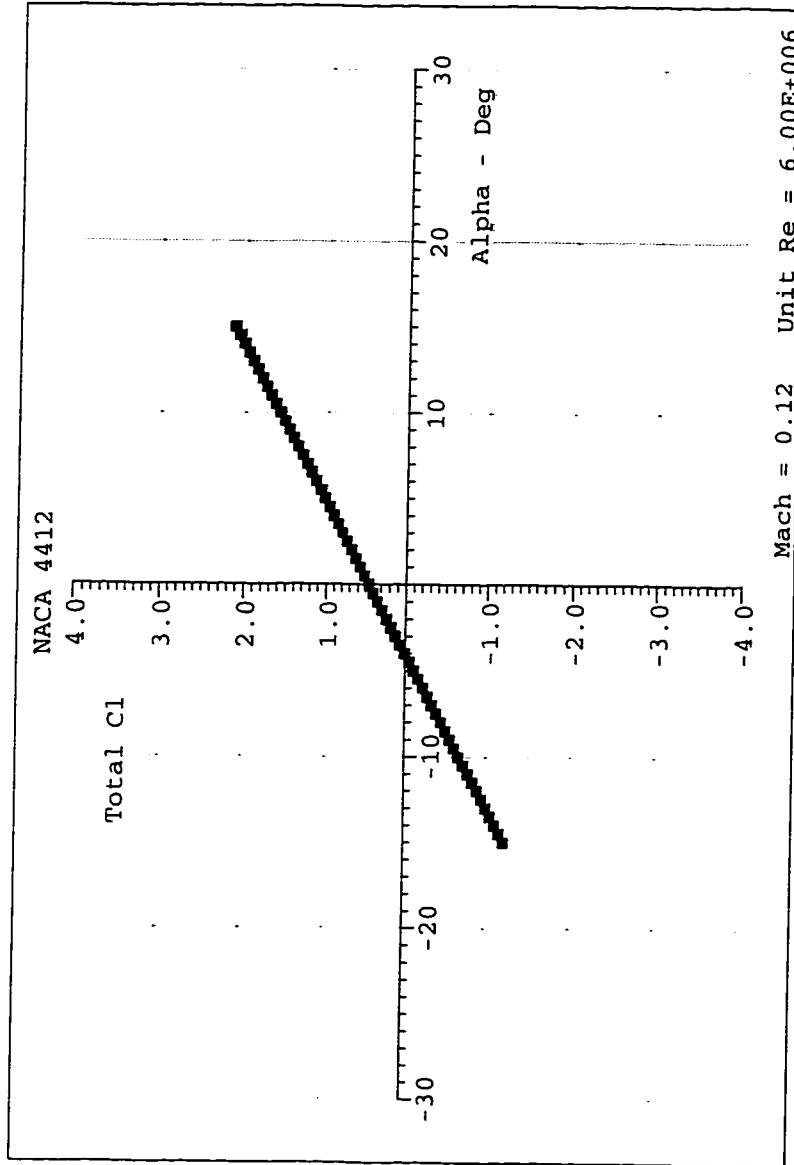


Fig. 9.3: Sub2D Output -  $C_l$  vs.  $\alpha$  at  $M = 0.12$

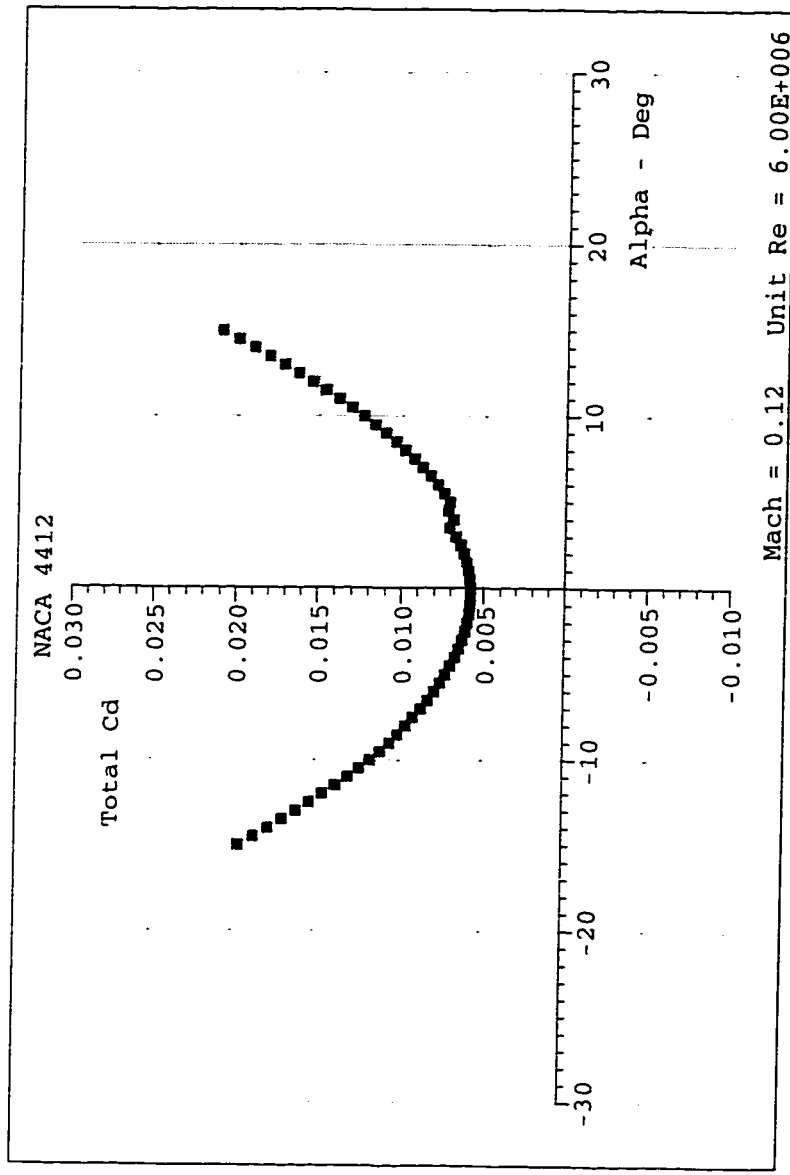


Fig. 9.4: Sub2D Output -  $C_d$  vs.  $\alpha$  at  $M = 0.12$



## Appendix A

### LabVIEW Functions

#### General Use Functions

AC & DC Estimator  
Amp & Freq Estimate  
Amplitude and Phase Spectrum  
Auto Power Spectrum  
Cross Power Spectrum  
Harmonic Analyzer  
Impulse Response Function  
Network Functions (avg)  
Power & Frequency Estimate  
Scaled Time Domain Window  
Spectrum Unit Conversion  
Transfer Function

#### Signal Generation

Arbitrary Wave  
Chirp Pattern  
Gaussian White Noise  
Impulse Pattern  
Periodic Random Noise  
Pulse Pattern  
Ramp Pattern  
Sawtooth Wave  
Sinc Pattern  
Sine Pattern  
Sine Wave  
Square Wave  
Triangle Wave  
Uniform White Noise

#### Windows

Blackman Window  
Blackman-Harris Window  
Cosine Tapered Window  
Exact Blackman Window  
Exponential Window  
Flat Top Window  
Force Window  
General Cosine Window  
Hamming Window  
Hanning Window  
Kaiser-Bessel Window  
Triangle Window

#### Filters

Bessel Filter  
Butterworth Filter  
Cascade->Direct Coefficients  
Chebyshev Filter  
Elliptic Filter  
Equi-Ripple Filter  
FIR Filter  
FIR Narrowband Filter  
FIR Windowed Filter  
IIR Cascade Filter  
IIR Filter with I.C.  
IIR Filter  
Inverse Chebyshev Filter  
Median Filter  
Parks-McClellan

#### Statistics

1D, 2D, and 3D ANOVA  
Chi Square Distribution  
Contingency Table  
erf(x)  
erfc(x)  
F Distribution  
General Histogram  
Histogram  
Inv Chi Square Distribution  
Inv F Distribution  
Inv Normal Distribution  
Inv T Distribution  
Mean  
Median  
Mode  
Moment about Mean  
MSE  
Normal Distribution  
Polynomial Interpolation  
Rational Interpolation  
RMS  
Spline Interpolant  
Spline Interpolation  
Standard Deviation  
T Distribution  
Variance

## Signal Processing

AutoCorrelation  
Complex FFT  
Convolution  
Cross Power  
CrossCorrelation  
Decimate  
Deconvolution  
Derivative  $x(t)$   
Fast Hilbert Transform  
Fast Hartley Transform  
Integral  $x(t)$   
Inverse Complex FFT  
Inverse Fast Hilbert Transform  
Inverse FHT  
Inverse Real FFT  
Peak Finding  
Power Spectrum  
Pulse Parameters  
Real FFT  
Threshold Peak Detector  
Unwrap Phase  
 $Y[i]=\text{Clip}\{X[i]\}$   
 $Y[i]=X[i-n]$   
Zero Padder

## Regression

Exponential Fit  
General LS Linear Fit  
General Polynomial Fit  
Linear Fit  
Nonlinear Lev-Mar Fit

## Array & Numeric

1D and 2D Linear Evaluation  
1D Polar To Rectangular  
1D and 2D Polynomial Evaluation  
1D Rectangular To Polar  
Numeric Integration  
Polar To Rectangular  
Quick Scale 1D and 2D  
Rectangular To Polar  
Scale 1D and 2D  
Find Polynomial Roots

## Linear Algebra

A x B  
A x Vector  
Determinant  
Dot Product  
Inverse Matrix  
Linear Equations

Normalize Matrix  
Normalize Vector  
Outer Product  
Trace  
Unit Vector  
LU Factorization  
Cholesky Factorization  
QR Factorization  
SVD Factorization  
Solve Linear Equations (extra input called by Linear Equations)  
EigenVectors and Values  
Matrix Condition Number  
Matrix Norm  
Matrix Rank  
PseudInverse Matrix  
Complex LU Factorization  
Complex Cholesky Factorization  
Complex QR Factorization  
Complex SVD Factorization  
Complex Inverse Matrix  
Solve Complex Linear Equations  
Complex EigenVectors and Values  
Complex Determinant  
Complex Matrix Condition Number  
Complex Matrix Norm  
Complex Matrix Rank  
Complex PseudInverse Matrix  
Complex A x B  
Complex A x Vector  
Complex Dot Product  
Complex Outer Product  
Complex Vector Norm  
Generate a Special Matrix

## Appendix B

### LabVIEW Manual for AE 162 Laboratory

#### Introduction to LabVIEW for Students

For the purposes of this lab only the basic run mode utilities will be described. For more information, read chapter 2 of the LabVIEW Data Acquisition VI Reference Manual and the LabVIEW Tutorial for Windows

LabVIEW is a programming language that uses icons to program the interface and the logical operation. VI is equivalent to a compiled ready-to-run program and is the terminology that LabVIEW uses to describe its executable files.

There are two screens available for every VI: The *Panel* window which contains what the user sees during operation and the *Diagram* window which contains the block diagram with the control algorithms that are involved in the setup.

Every LabVIEW display contains the following buttons:

From the “Run Mode” palette:



Single run button. Runs only one cycle of the programmed setup



Run/Edit mode button (shown in “Run” mode)



Run/Edit mode button (shown in “Edit” mode)



Continuous run button. Cycles through the program until the user selects *STOP*



Stop button. Stops data updating after the *Continuous run* button is activated



Step through button. Displays each sequence with all subcomponents during runtime in the *Diagram* window

To start data acquisition press the *Continuous run* button. This starts all processes that are programmed in the block diagram in the *Diagram* window available from the *Windows* menu. To stop the process press the *Stop* button.

You must click on the *Stop* button before editing either the front panel or the diagram.

## Starting LabVIEW

1. Turn on the power strip. This will turn on the computer, monitor, terminal box, sensor power supply and the ELD console.
2. Start Microsoft Windows: **win** ↵
3. When Windows starts, if the LabVIEW window is already open, double-click on the LabVIEW icon. If not, double click on the LabVIEW file icon first.
4. Typically, you will first see an “Untitled 1” window. Hit **Control-W** to close the window.
5. Select “Open VI” from the new window.
6. Double-click on the “AE-162” folder and then select the proper VI to start. Notice the directory “TEST\_DIR”. It contains test setups for various calibrations and experimental setups, but no user editable files.

As of 4/97 there are three VIs available:

- **CONSOLE.VI** Displays all of the information you can see by turning the “Signal Selector” knob on the console. Also performs various calculations such as  $L/D$ , velocity at pitot tube etc.
- **CP4412.VI** Displays  $C_p$  for upper and lower surfaces of the NACA 4412 airfoil. Also displays velocity at pitot tube.
- **VEL-PROF.VI** Displays the pitot tube velocity at specific locations.

All main displays have instructions for setting calibration and reference constants. Read each screen carefully, otherwise your data maybe inaccurate.

To quit LabVIEW hit **Control-Q** at any time.